Viscous-Inviscid Methods in Unsteady Aerodynamic Analysis of Bio-Inspired Morphing Wings

by Akash V. Dhruv

B. Tech in Mechanical Engineering, October 2013, National Institute of Technology, Surat

A Thesis submitted to

The Faculty of
The School of Engineering and Applied Science
of the George Washington University
in partial fulfillment of the requirements
for the degree of Master of Science

August 31, 2015

Thesis directed by

Adam M. Wickenheiser
Assistant Professor of Engineering and Applied Science

© Copyright 2015 by Akash V. Dhruv
All rights reserved

Dedication

To my parents, my inspiration. Thank you for giving me my wings.

Acknowledgments

I want to take this opportunity to thank everyone who has supported me throughout the process of this research. Professor Adam Wickenheiser, who gave me the opportunity to work on the project and provided me with helpful advice both technically and academically. Chris Blower, who has been a great mentor since the day we started our research together. My friends, Prithvi and Anuja who always made me see the brighter side of the things, and to my room-mates and loved ones for finally making peace with my eccentric behavior during this whole process of writing.

I was fortunate to undertake my courses under distinguished Professors, who have inspired me to accept difficult challenges and tackle them head-on. I would also like to thank SEAS for providing me with the facilities to work on my research and the Gelman Library and its staff for working hard to keep the library open for 24 hours. They both have been a second home to me.

Lastly, I would like to thank my parents, Hina and Vijay Dhruv for believing in my dreams and to Soumya and Pooja for inspiring me when I was down.

Abstract

Viscous-Inviscid Methods in Unsteady Aerodynamic Analysis of Bio-Inspired Morphing Wings

Flight has been one of the greatest realizations of human imagination, revolutionizing communication and transportation over the years. This has greatly influenced the growth of technology itself, enabling researchers to communicate and share their ideas more effectively, extending the human potential to create more sophisticated systems. While the end product of a sophisticated technology makes our lives easier, its development process presents an array of challenges in itself. In last decade, scientists and engineers have turned towards bio-inspiration to design more efficient and robust aerodynamic systems to enhance the ability of Unmanned Aerial Vehicles (UAVs) to be operated in cluttered environments, where tight maneuverability and controllability are necessary. Effective use of UAVs in domestic airspace will mark the beginning of a new age in communication and transportation.

The design of such complex systems necessitates the need for faster and more effective tools to perform preliminary investigations in design, thereby streamlining the design process. This thesis explores the implementation of numerical panel methods for aerodynamic analysis of bio-inspired morphing wings. Numerical panel methods have been one of the earliest forms of computational methods for aerodynamic analysis to be developed. Although the early editions of this method performed only inviscid analysis, the algorithm has matured over the years as a result of contributions made by prominent aerodynamicists. The method discussed in this thesis is influenced by recent advancements in panel methods and incorporates both viscous and inviscid analysis of multi-flap wings. The surface calculation of aerodynamic coefficients makes this method

less computationally expensive than traditional Computational Fluid Dynamics (CFD) solvers available, and thus is effective when both speed and accuracy are desired. The morphing wing design, which consists of sequential feather-like flaps installed over the upper and lower surfaces of a standard airfoil, proves to be an effective alternative to standard control surfaces by increasing the flight capability of bird-scale UAVs. The results obtained for this wing design under various flight and flap configurations provide insight into its aerodynamic behavior, which enhance the maneuverability and controllability. The overall method acts as an important tool to create an aerodynamic database to develop a distributed control system for autonomous operation of the multi-flap morphing wing, supporting the use of viscous-inviscid methods as a tool in rapid aerodynamic analysis.

Table of Contents

Title Page i

Dedication iii

Acknowledgments iv

Abstract v

Table of Contents vii

List of Figures ix

Chapter 1: Introduction 1

1.1 Thesis Overview 1

1.2 Multi-Flap Wing Design 3

Chapter 2: Literature Review 6

2.1 A Brief History of Panel Methods 6

2.2 Panel Method Algorithms 8

Chapter 3: Methods 12

3.1 Two-Dimensional Panel Method 12

3.1.1 Constant Strength Doublet Panel Method 15

3.1.2 Constant Strength Doublet-Source Panel Method 18

3.2 Wake Relaxation and Discretized Wake Method 20

3.3 Three Dimensional Panel Method 26

3.4 Unsteady Panel Methods 29

3.5 Vortex Particle Method 33

3.6 Viscous Formulation 36

Chapter 4: Results 40

4.1 Validation 40

4.2 Aerodynamic Behavior of Multi-Flap System 50

Chapter 5: Conclusion 58

References 60

Appendix A: Differential Evolution Algorithm 63

List of Figures

Figure 1: Bio-Inspired Multi-Flap System..... 2

Figure 2: MFS configurations (a) Rest configuration (b) Lifting configuration..... 4

Figure 3: MFS configurations (a) Stall avoiding (b) Air-braking..... 4

Figure 4: Three dimensional wing consisting of three MFS wing sections..... 5

Figure 5: Discretrization of airfoil geometries into panels (a) NACA 4412 Airfoil (b) Bio-Inspired Multi-Flap System..... 8

Figure 6: Geometry for panel method: end points (black dots) and collocation points (blue *)..... 13

Figure 7: Airfoil and wake geometry..... 15

Figure 8: Discretized wake profile for wake relaxation..... 24

Figure 9: Wake profiles computed using different assumptions: free stream-aligned wake (blue), trailing edge bisector-aligned wake (red), and discretized wake panel relaxation scheme (green)..... 26

Figure 10: NACA 4412 wing geometry for validating the panel method, with an aspect ratio of 5. The cutting plane shows the mid-span section where C_p values are compared with two dimensional results..... 27

Figure 12: Initial Geometry for unsteady panel method with buffer wake panel..... 31

Figure 13: Wake roll up and C_p distribution achieved at the steady state for NACA 4412 wing with an aspect ratio of 5 and $\alpha = 0^\circ$ 32

Figure 14: (a) Discretized wakes shed from trailing edge of flaps following the local velocity vectors when the distances between flaps are comparable to wake panel lengths. (b) Wakes violating non permeability boundary condition when distance between sequential flaps is smaller in comparison to wake panel lengths... 34

Figure 15: (a) Vortex particle wake shed behind a NACA 0012 wing with an aspect ratio of 5 and α=5°. (b) Wake roll behind two-element airfoil using vortex particles (Wing- NACA 4412, Flap- NACA 4415), α=0°..... 36

Figure 16. Boundary layer over a NACA 0012 airfoil at Re = 6,000,000..... 39

Figure 17: Coefficient of Pressure comparison for different wake profiles for NACA 4412 at angle of attack 13.87^o..... 41

Figure 18: Coefficient of Pressure comparison obtained by different methods for NACA 4412 at angle of attack 13.87^o..... 41

Figure 19: Variation of coefficient lift with respect to the panel density using a doublet source panel method over a NACA 4412 airfoil, angle of attack 0^o..... 42

Figure 20: Validation of a single element 3D panel method in comparison to 2D panel method and experimental results [11, 12]. Aspect Ratio = 100, number of chord-wise panels = 40 and span-wise panels = 100,α=13.87°..... 43

Figure 21: Validation of 3D panel method with XFLR5 for a NACA 4412 wing with an aspect ratio of 10 and α=10..... 44

Figure 22: Two Element Airfoil (Wing NACA-4412 c=1.0) (Flap NACA-4415 c=0.5, deflection=21°)..... 45

Figure 23: Comparison of 2D and 3D panel method (a) at aspect ratio = 5 (b) at aspect ratio = 20 and α=8.2°, showing how high aspect ratio wings behave like a 2D airfoil..... 46

Figure 24: (a) Coefficient of Pressure at the mid section of NACA 4412 wing with the Aspect Ratio of 5 at α=0° at different time step (b) Comparison of the Results of Unsteady 3D Panel Method obtained at the steady state with that of the Steady 3D Panel Method for a NACA 4412 wing with an Aspect Ratio of 5 at α=0°..... 47

Figure 25: (a) Discretized wake method fails when flap distance are lesser than the wake panel lengths (b) Unrealistic pressure profile is obtained when wakes pass through the body of the flaps (c) Vortex particle method resolves wake profiles for configurations when flap distance are ~.002c resulting in accurate assessment of the aerodynamic coefficients..... 48

Figure 26: Comparison of Coefficient of Pressure obtained by a vortex particle method and unsteady panel method (each wake panel is represented by two vortex particles)..... 49

Figure 27: (a) Bio-inspired multi-flap system geometry with two span-wise systems of flaps (station 1 and station 2) with mid-span positions where C_p is

calculated for aspect ratio=4 with all deflections set to 0°. (b) Coefficient of pressure plots at mid-span positions for both station 1 and 2 (black upper flaps and leading edge, red-lower flaps, green- NACA 4412), α=10°, aspect ratio=4..... 51

Figure 28: (a) Bio-inspired multi-flap system geometry with three span-wise systems of flaps and aspect ratio=6 with deflections
(b) Coefficient of pressure plots at mid-span positions for all the three stations α=10°, aspect ratio=6..... 52

Figure 29: Vortex particle wake behind multi-flap system configuration for air braking..... 53

Figure 30: Bio-Inspired Multi-Flap Configuration to delay separation and avoid gust, α=10°..... 54

Figure 31: Rest configuration for cruise flight, all flap deflections are zero..... 55

Figure 32: Clockwise roll..... 55

Figure 33: Counter- clockwise roll..... 55

Figure 34: Air-Braking..... 55

Figure 35: Right-Yaw..... 56

Figure 36: Left-Yaw..... 56

Figure 37: Gust-alleviation at high angle of attack..... 56

Figure 38: A UAV incorporated with the Bio-Inspired Multi Flap System..... 59

Figure 39: Different configurations of the leading edge of the Multi-Flap System.... 63

Chapter 1- Introduction

1.1 Thesis Overview

Morphing wings are a class of wings that can modify their shape during flight, generating different aerodynamic profiles. In recent years, scientists and engineers have turned towards bio-inspiration to design this type of wing to increase maneuverability of bird-scale UAVs in cluttered environments. The inability of traditional fixed-wing aircraft to negotiate around obstacles and withstand gusting flows has presented challenges in the operation of UAVs in urban environments. This in turn has limited their use in modern transportation and communication [1-2]. Replacing traditional control surfaces such as flaps and ailerons with morphing wings not only improves the aerodynamic performance of these aircraft but also enhances their stability and controllability while performing complex maneuvers.

We have used the principle of morphing wings to develop a multi-flap system inspired by avian flow control characteristics. Birds deflect their feathers to manipulate local airflow while maintaining flight stability in cruise and at high angles of attack. Installing feather-like flaps over the surface of a standard airfoil that can deflect into the airfoil and outwards mimics this behavior. Fig 1 shows a Multi-Flap System with 8 flaps over upper and lower surfaces following a standard NACA 4412 airfoil profile.

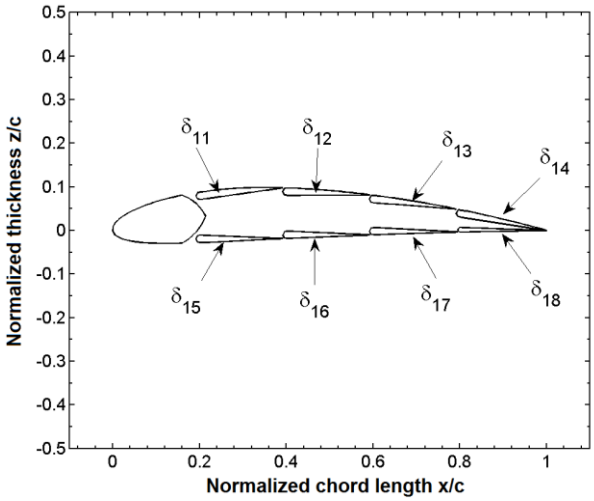

Figure 1: Bio-Inspired Multi-Flap System. While in the rest configuration, the outer surfaces of the flaps conform to a NACA 4412 airfoil.

This two-dimensional profile can be extended into three dimensions to generate a Multi-Flap Wing that can produce complex aerodynamic profiles to control the motion of a UAV in the longitudinal and lateral directions.

Since the deflection of flaps depend upon the flight conditions and the required maneuver, a robust unsteady aerodynamic solver is needed to rapidly calculate the coefficients over the surface of the flaps; thus, a viscous-inviscid panel method solver is developed. The advantage of using a viscous-inviscid panel method over computational methods lies in the fact that the former solves the flow over the surface of the wing instead of calculating the complete flow field, thereby reducing a three-dimensional problem to a two-dimensional one or a two-dimensional problem to a one-dimensional one. This decreases the number of computations significantly for a given problem and thus increases the speed of the solver.

When considering the aerodynamic analysis of morphing wings, the wake-body interaction plays an important role. An accurate wake shape not only ensures that the

necessary boundary conditions are satisfied, but also increases the accuracy of the results. The panel method algorithm for multi-flap wings thus needs to be modified to model these interactions and incorporate wake relaxation to orient wake panels along the local flow velocities. The research undertaken in this thesis discusses implementation of discretized and vortex particle wakes to integrate wake dynamics into the traditional panel method code. The complete viscous-inviscid formulation consists of augmenting this modified panel method code with a boundary layer model.

The complete solver serves as an important simulation tool for bio-inspired wings and is faster than the existing solvers available for preliminary aerodynamic analysis.

1.2 Multi-Flap System (MFS) Design

The multi-flap morphing wing system changes the airfoil shape by deflection of flaps. In their rest configuration, these flaps follow the profile of a standard NACA 4412 airfoil, which has been extensively analyzed and researched both experimentally and numerically. The outer surfaces of the flaps follow the airfoil profile and the inner surfaces are modeled such that each flap is a symmetric airfoil. The leading edge of the system is treated as a bluff body and its design was optimized using a differential evolution algorithm such that its aerodynamic behavior is similar to that of the leading edge of the NACA 4412 wing. This is done by taking the difference between the pressure distributions obtained for MFS and NACA 4412 as a cost function and minimizing it until the required cost criteria is met. The algorithm for differential evolution is given in Appendix A.

As discussed earlier, different flap configurations generate different aerodynamic profiles. For example, the deflection of trailing edge flaps at a negative angle, as shown in Fig. 2b, increases the total lift over the surface of the airfoil.

(a) (b)

Figure 2: MFS configurations (a) Rest configuration (b) Lifting configuration

Shown in Fig. 3(a), if the flaps are deflected slightly outwards, then the trailing edge vortices shed from each flap reattach the separated flow when operating at higher angle of attack. Deflecting the flaps further outwards increases the drag on the airfoil and thus can be used for air braking, as shown in Fig. 3(b).

(a) (b)

Figure 3: MFS configurations (a) Stall avoiding (b) Air-braking

While operating in gusting environments, the flaps can be oriented along the flow direction, which causes the pressure gradient over each flap surface to oppose the adverse pressure gradient and thus maintain aerodynamic stability.

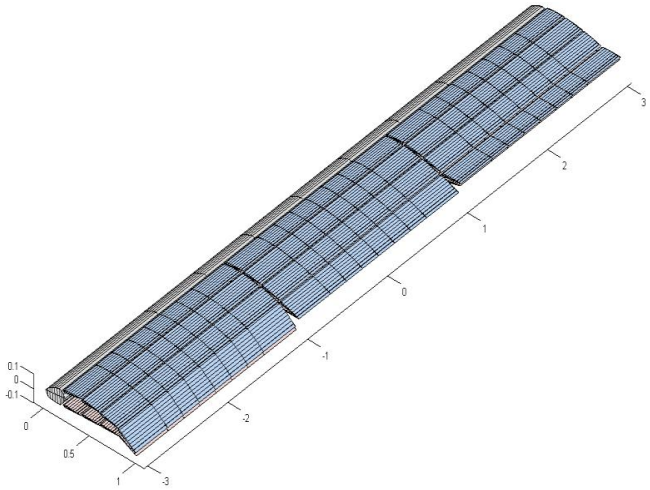

Figure 4: Three dimensional wing consisting of three MFS wing sections

The three-dimensional application of the MFS can be achieved by installing the airfoil cross-section at different locations along the span. For example, Fig. 4 shows a multi-flap wing with three flap stations. Each flap station behaves independently, and a combination of different configurations generates the required aerodynamic motions.

The following chapters discuss the implementation of a robust aerodynamic solver to analyze the configurations discussed above and handle wake-body interactions during unsteady flow conditions. The solver then can be used to create an aerodynamic database to develop a distributed control system for autonomous operation of the UAV.

This design serves to replace the existing control mechanisms on bird-scale UAVs and improve their ability to operate in urban environments, paving the way for their use in agriculture, traffic monitoring, package delivery, security and surveillance. This in turn will contribute towards better communication and transportation, enabling faster exchange of ideas and information.

Chapter 2- Literature Review

2.1 A Brief History of Panel Methods

During the 1950s, high performance computing was a relatively new concept. Although significant contributions had been made which would later influence the computing power in the 21st century, solving Navier-Stokes equations rapidly, using parallel programming was a dream yet to be recognized. The research in Computational Fluid Dynamics (CFD) was limited by the availability of these resources, and aerodynamicists still used primitive methods to analyze flow over aircraft and complex multi-element wings (the most popular method involved converting an aircraft configuration into a body of revolution using Richard Whitcomb's area rule [3]). The results produced from these methods were far from accurate because converting a complete aircraft to an equivalent body of revolution leads to a bumpy geometry thereby resulting in incorrect values of aerodynamic coefficients [3]. These deficiencies helped motivate the development of early panel method solvers.

The earliest contributions to the panel methods were made by Hess and Smith of Douglas aircraft company [3]. In 1952, Smith started his work on developing a Neumann method to solve potential flow aerodynamics equations over the surface of an aircraft. This method would be later named a panel method because of the way it treated the surface geometry of wing/aircraft by dividing it into flat quadrilateral panels. The idea is to model the flow over the surface by superimposing a set of singularity solutions like sources. Each panel represents a constant source density of strength σ, which induces velocities on the other panels. The total velocity induced on each panel obeys the no-flow

Neumann boundary condition and models the tangential flow over the surface. The early versions of this method were programmed in machine language using an IBM/701. The results obtained from this method were considerably accurate compared to the previous methods, and further extensions were made to solve for multi-element wings and two-dimensional lifting flows.

Over the years, improved versions of then established panel methods were developed that used different singularity solutions like doublets and vortices and included the addition of a trailing edge Kutta condition to solve for lifting airfoils [4-10]. The most significant contribution was the VSAERO program developed by NASA, which modeled the wake and the body using discretized doublet and source panels [7,10]. The discretized wake representation increased the accuracy of results, which is discussed in detail in Section 4.1.

The late 20^{th} century marked an increase in availability of computational resources. Although inviscid panel methods were a popular tool for preliminary aerodynamic analysis, CFD, now a mature field, became a more popular tool for detailed analysis of flows. However, researchers continued to improve upon existing panel method by incorporating viscous and boundary layer models to simulate complex flows. Katz, Plotkin and Drela pioneered the research in this field during this era by exploring different aspects of panel methods in unsteady aerodynamic analysis and developing software like XFOIL, which is still used today by many researchers [11].

Over the next few years, the general interest in panel method waned, as more focus was given on developing high fidelity CFD solvers. This era marked an increased focus in

parallel programming and development of higher level, object oriented languages, which facilitated the development of computational science. The availability of high performance computing resources for commercial use allowed researchers and students alike to explore the regimes of high Reynolds number turbulent flows, establishing CFD as one of the most reliable tool for fluid dynamic analysis.

The development of MAVs and UAVs over the last decade has led to design of bio-inspired wings. This has led researchers to revisit panel method algorithms and improve upon them as a faster alternative to solve viscous-inviscid equations simultaneously. Computational techniques like vortex particle methods [12] have been integrated into these models to replace the discretized wake representation, facilitating a decrease in user effort to implement this method in analysis of complex structures like multi-flap, morphing wings.

2.2 Panel Method Algorithms

The basic formulation of the two-dimensional panel method developed by Hess and Smith [7-10] consists of dividing the airfoil and wake geometry into line-segments called panels as shown in Fig 5(a).

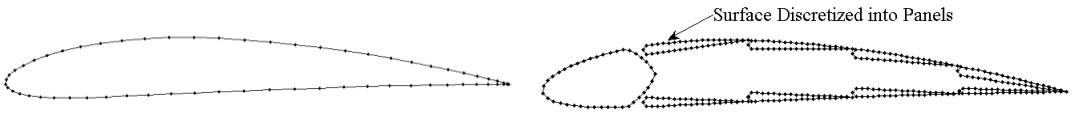

(a) (b)

Figure 5. Discretrization of airfoil geometries into panels (a) NACA 4412 Airfoil (b) Bio-Inspired Multi-Flap System

To model the flow over the surface of this airfoil, constant strength doublet and source singularities are assumed to be located on the collocation points (mid points) of these panels. Each doublet and source singularity induces velocities at every collocation point,

resulting in a system of linear equation. The superimposition of all singularities simulates the inviscid flow over the surface of the wing. This is the simplest version of the method, consisting of only one wake panel along the free stream extending to infinity downstream (truncated to twenty times the chord length) and thus is suitable when considering single- or two-element formulation. When the length of the wake reaches twenty times the chord length, disturbances induced by the presence of the wing are assumed to have been dispersed since the influence of singularities is inversely proportional to the distance away from them. However, when extending this method to multiple bodies like the morphing wing discussed in Section 1.2, a single wake panel model fails. This is because representing the wake with just one panel makes it inflexible, and thus it cannot align itself to local free-stream velocity.

When simulating flow over a multi-body wing, as shown in Fig 5(b), the single wake panel from a leading flap may pass through the body of a flap located aft of the former, violating the impermeability boundary condition. Thus the basic panel method can be improved by using a discretized wake panel, as discussed by Bramesfeld [11] and implemented in VSAERO [10]. This method considerably improves the panel method algorithm to simulate flow over multi-body wings. The discretized wake panels are aligned to the local flow velocity by calculating the velocity induced on them and reorienting their positions.

The discretized wake model is an improvement on the original panel method model, but it requires the user to define an initial wake profile. This adds complexity to the algorithm because a standard initial wake shape may not be suitable for all flap configurations, and thus the user has to change the wake geometry for each configuration such that the

impermeability boundary condition is not violated. This problem can be tackled by using an unsteady formulation as discussed by Katz [7]. In this formulation, the user only needs to define the wing geometry and a set of single buffer wake panels extending from the trailing edge of each flap. The length of this wake panel is set equal to $CU\Delta t$ Where, U is the magnitude of the free stream velocity, Δt is the time step of the unsteady formulation and C is a numerical constant [7]. As the time steps progress, discretized wake panels are added along the local flow velocity aft of the buffer wake panel. The simulation continues until the wake length reaches the required value of ten times the chord length. The flow disturbances due to wing are assumed to have been dispersed at this distance, and the wake is assumed to have merged with the free-stream [7-13]. For unsteady cases, the simulation progresses until the required time is reached.

The complete unsteady panel algorithm method now can be incorporated with a boundary layer model to include the viscous effects over the surface of the airfoil. Various methods have been developed that solve the boundary layer and inviscid formulation simultaneously using a Newton-Raphson method. One such method developed by Giles and Drela consists of integrating a doublet source panel method with integral boundary layer equations [7]. The accuracy of the solver can be improved by using the differential form of the boundary layer equations and solving them over a grid, as discussed by Morino [24].

The unsteady panel method is a great tool for aerodynamic analysis. It reduces the user effort to define wake geometry and solves for both steady and unsteady flows. However, this method fails when the distances between flaps are smaller than the wake length. This problem can be avoided by either decreasing the time step or using a vortex particle

method to represent the wake as discussed by Willis et al. and Winckelmans [16-18]. The vortex particle formulation consists of collapsing the doublet buffer wake panels from the previous time step into vortex particles of equivalent strengths and then advecting them into the domain. This further simplifies the method in terms of wake-body interactions since each vortex wake particle behaves independently and is not confined to a specified wake geometry as in the case of discretized wake methods.

The vortex particle method is more computationally expensive than a discretized wake method because more than one vortex particle is required to represent a doublet sheet. However, it is suitable for configurations where flap distances are very close to each other. For the bio-inspired wing considered in this thesis, a combination of both methods is suitable.

Chapter 3- Methods

This chapter discusses the mathematical model of the viscous-inviscid algorithm for bio-inspired morphing wings. Starting from the basic formulation, complexities are added to the method to effectively simulate the flow over multi-flap morphing wings. The simplest form of the algorithm is a two-dimensional doublet-source panel method for single-element wings. This algorithm can easily be extended to solve for multi-flap wings in which the wakes from different flaps have little interaction. To enable accurate simulation of flows over the wing, a wake relaxation algorithm is implemented, which uses a discretized wake to align wake panels along the local velocity direction. The complete method is then supplemented with an integral boundary layer model to complete the viscous-inviscid analysis.

To reduce the user effort to define wake geometries for multi-flap wings, a mathematical formulation of an unsteady panel method is also discussed. To improve the performance of this method a vortex particle wake is later implemented.

3.1 Two Dimensional Panel Method

To understand the mathematical formulation of the two dimensional panel method, consider the airfoil geometry shown in Fig 6.

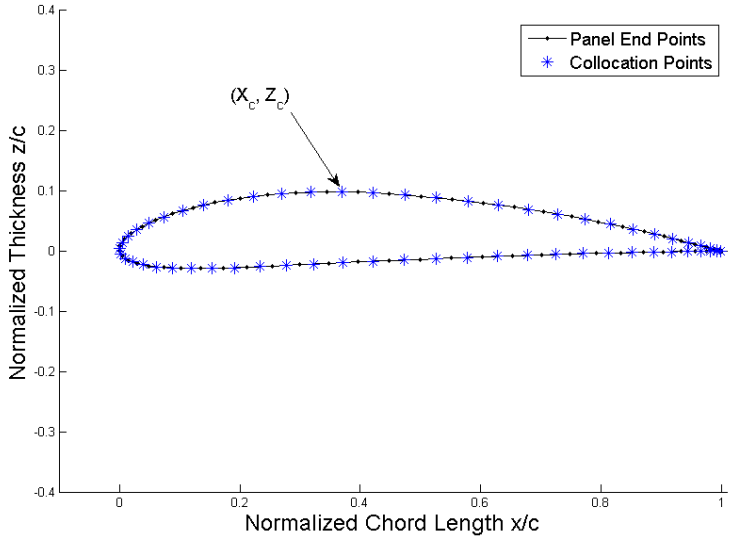

Figure 6: Geometry for panel method: end points (black dots) and collocation points (blue *)

This smooth surface geometry is first divided into line segments called panels. The end points of these panels are arranged in a continuous array from lower surface to the upper surface starting from the trailing edge of the airfoil. Once this is complete, the mid-points of these panels are calculated and stored in a separate array; these points are termed collocation points because the boundary conditions are evaluated at these points. Constant strength singularity solutions are assumed to be located at each collocation point. The strengths of these singularities are unknown ahead of time. The purpose of the solver is to find these unknown strengths and superimpose them to simulate the flow over the surface of the airfoil.

Each singularity element induces a velocity at every point in the domain, particularly at the collocation points on the surface of the airfoil. The total velocity at a given point is the vector sum of the velocities induced by all of the singularities and the free stream. For example, consider a collocation point given by (x_c, z_c) in Fig 6. The total velocity induced at this point is the sum of the velocities induced by the unknown singularities at

each collocation point (including the given point itself) and the free stream. This forms the left-hand side of the system of equations. Since the doublet strengths are unknown, we need a right hand side condition to form a system of linear equations. This right hand side is obtained by imposing the impermeability boundary condition on the surface of the airfoil. This is popularly known as a Neumann boundary condition, which states that the normal flow through the surface of the airfoil is zero. This condition, when imposed at all the collocation points that define the airfoil, results a system of linear equations. This system can then be solved to obtain the unknown strengths of the singularities, thus simulating the inviscid flow over the airfoil. Alternatively, a Dirichlet boundary condition can also be used when considering the aerodynamic analysis of thick airfoils. This condition states that the potential ϕ inside the body of the airfoil is considered to be zero. This simplifies the problem because the velocity potential is a scalar quantity, and thus the complexities associated with vector summation of the velocities are avoided.

Another important aspect of the panel method is the imposition of the Kutta condition, which states that bodies with sharp trailing edges induce circulation around themselves to maintain the stagnation point at the trailing edge. In a physical sense, the Kutta condition means that the velocities at the upper and lower surfaces of the airfoil should be parallel to each other at the trailing edge. This is mathematically modeled by considering a wake panel extending from the trailing edge up to infinity (twenty times the chord length). The singularity strength of this wake panel is dependent on the singularity strengths of the upper and lower trailing edge panels.

The choice of singularity element is an important aspect of the panel method. Ideally, singularity solutions like vortices or doublets are chosen to simulate the lifting flow. If

the flow is modeled using only source singularities then it would be a non-lifting one. This is because circulation cannot be modeled using only sources. A combination of either vortex-source or doublet-source singularities is a better approach because doublets and vortices model the lifting flow and sources model the boundary layer by accounting for mass defect in the boundary layer equations. This algorithm is discussed in the following sections, where the complete viscous-inviscid formulation is developed using a doublet source method. There have been no substantial arguments claiming that doublets are a better choice over vortices. On the contrary, the formulation of the different methods discussed by Katz [7] proves that a doublet and vortex panel method are mathematically equivalent.

3.1.1 Constant Strength Doublet Panel Method

Before proceeding towards the doublet-source method used in this thesis, the doublet formulation is developed first. This is good starting point for someone who wants to learn the basics of numerical methods in potential flow aerodynamics since it serves as a stepping stone for more complex methods.

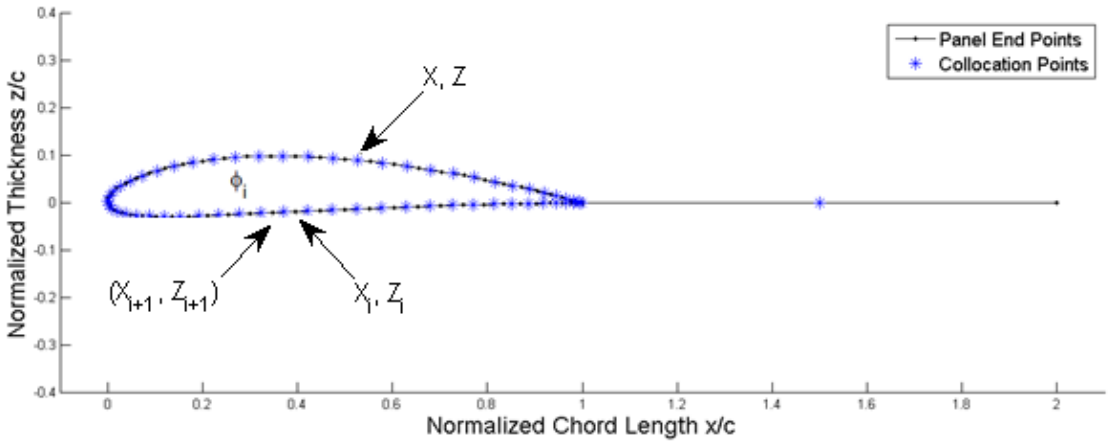

Figure 7: Airfoil and wake geometry

Consider an airfoil with *N* panels, *N* collocation points, *N+1* panel end points and one wake panel, as shown in Fig 7. The unknown doublet strengths μ are located on every collocation point. Each doublet induces a velocity potential on every collocation point given by

$$\phi_d = \frac{-\mu}{2\pi}\left[\tan^{-1}\frac{z_c}{x_c - x_p} - \tan^{-1}\frac{z_c}{x_c - x_0}\right] \text{ (panel coordinates)} \qquad (1)$$

where (x_0, z_0) and (x_p, z_p) are panel end points and (x_c, z_c) is panel collocation point in the panel coordinate system, which is related to the global coordinate system by the equation

$$\begin{bmatrix} x_p \\ z_p \end{bmatrix} = \begin{bmatrix} \cos\alpha_i & -\sin\alpha_i \\ \sin\alpha_i & \cos\alpha_i \end{bmatrix}\begin{bmatrix} x_{i+1} - x_i \\ z_{i+1} - z_i \end{bmatrix}$$

$$\begin{bmatrix} x_0 \\ z_0 \end{bmatrix} = \begin{bmatrix} \cos\alpha_i & -\sin\alpha_i \\ \sin\alpha_i & \cos\alpha_i \end{bmatrix}\begin{bmatrix} x_i - x_i \\ z_i - z_i \end{bmatrix} \qquad (2)$$

$$\begin{bmatrix} x_c \\ z_c \end{bmatrix} = \begin{bmatrix} \cos\alpha_i & -\sin\alpha_i \\ \sin\alpha_i & \cos\alpha_i \end{bmatrix}\begin{bmatrix} x - x_i \\ z - z_i \end{bmatrix}$$

Here, (x_i, z_i), (x_{i+1}, z_{i+1}) are the panel end points and (x, z) is the panel collocation point in the global coordinate system and α_i is the panel angle of attack.

The Dirichlet boundary condition states that the velocity potential inside a closed body is constant. In Fig. 7,

$$\phi_i = const. \qquad (3)$$

To obtain a unique solution to this problem the value of the constant must be specified and is taken to be zero. Furthermore, this internal potential can be defined as the combination of the potential ϕ_d induced by the doublet singularities and the potential ϕ_∞ induced by the free-stream flow, resulting in the equation

$$(\phi_d + \phi_\infty) = 0 \tag{4}$$

Where, $\phi_\infty = U_\infty x + W_\infty z$ and (U_∞, W_∞) is the free-stream velocity.

Since the doublet strengths on the collocation points are initially unknown, an influence matrix is created using $\mu = 1$ in Eq. (1). This is the unit influence on the potential ϕ_d of a panel on a given collocation point, given by

$$C_{panel} = \frac{-1}{2\pi}\left[\tan^{-1}\frac{z_c}{x_c - x_p} - \tan^{-1}\frac{z_c}{x_c - x_0}\right] \text{ (panel coordinates)} \tag{5}$$

Eq. (4) now can be written as

$$\sum_{j=1}^{N} C_j \mu_j + \phi_\infty = 0 \tag{6}$$

Next the Kutta condition is satisfied explicitly. The doublet strength of the wake panel, μ_w is also an unknown and must satisfy the equation

$$\mu_1 - \mu_N + \mu_w = 0 \tag{7}$$

where μ_1 and μ_N are the doublet strengths of the lower and upper trailing edge panels, respectively.

The complete influence matrix thus becomes

$$\sum_{j=1}^{N+1} C_{ij}\mu_j = \begin{bmatrix} c_{11} & c_{12} & \ldots & c_{1N} & c_{1W} \\ c_{21} & c_{22} & \ldots & c_{2N} & c_{2W} \\ \ldots & \ldots & \ldots & \ldots & .. \\ c_{N1} & c_{N2} & .. & c_{NN} & c_{NW} \\ 1 & 0 & 0 & -1 & 1 \end{bmatrix} \begin{bmatrix} \mu_1 \\ \mu_2 \\ .. \\ \mu_N \\ \mu_W \end{bmatrix} \tag{8}$$

The influence of a panel on itself is given by $c_{ii} = \frac{1}{2}$ [7]. The resulting linear system of equation becomes

$$\begin{bmatrix} c_{11} & c_{12} & \ldots & c_{1N} & c_{1W} \\ c_{21} & c_{22} & \ldots & c_{2N} & c_{2W} \\ \ldots & \ldots & \ldots & \ldots & .. \\ c_{N1} & c_{N2} & .. & c_{NN} & c_{NW} \\ 1 & 0 & 0 & -1 & 1 \end{bmatrix} \begin{bmatrix} \mu_1 \\ \mu_2 \\ .. \\ \mu_N \\ \mu_W \end{bmatrix} + \begin{bmatrix} \phi_{\infty_1} \\ \phi_{\infty_2} \\ \\ \phi_{\infty_N} \\ 0 \end{bmatrix} = 0 \tag{9}$$

where, $\phi_{\infty_1}, \phi_{\infty_2}, ..., \phi_{\infty_N}$ are the velocity potential induced by the free-stream at collocation points. Solving this system of linear equation results in the unknown doublet strengths of the wake and the body panels. These strengths now can be used to calculate the induced velocity on all the collocation points thus simulating the inviscid flow over the airfoil.

3.1.2 Constant Strength Doublet-Source Panel Method

In this formulation, both source and doublet singularities are assumed at each collocation point. The sources induce the mass defect which model the boundary layer and the doublets model the inviscid part of the flow. The total velocity potential induced at each collocation point is the summation of the potentials induced by the doublets, sources and the free-stream. The resulting equation is given by

$$\phi_d + \phi_s + \phi_\infty = const. \tag{10}$$

where ϕ_s is the velocity potential induced by the source singularities. The influence of a unit source singularity is given by

$$B_{panel} = \frac{1}{4\pi}\left[(x_c - x_0)\ln[(x_c - x_0)^2 + z_c^2] - (x_c - x_p)\ln[(x_c - x_p)^2 + z_c^2 + 2z_c\left(\tan^{-1}\frac{z_c}{x_c - x_p} - \tan^{-1}\frac{z_c}{x_c - x_0}\right)\right] \tag{11}$$

(panel coordinates)

Thus, the complete system is given by

$$\sum_{j=1}^{N} C_j \mu_j + \sum_{j=1}^{N} B_j \sigma_j + \phi_\infty = 0 \tag{12}$$

Using sources along with doublets is useful when considering the complete viscous-inviscid interaction. The source strengths represent the mass-defect and thus account for the boundary layer thickness. For the initial inviscid analysis, however, the source strengths are calculated assuming the constant in Eq. (10) to be equal to ϕ_∞, which gives

$$\sigma_j = n_j . Q_\infty \tag{13}$$

where n_j is a unit vector normal to the panel, and Q_∞ is the free-stream velocity.

Finally, the system in matrix form is given by

$$\begin{bmatrix} c_{11} & c_{12} & \ldots & c_{1N} & c_{1W} \\ c_{21} & c_{22} & \ldots & c_{2N} & c_{2W} \\ \ldots & \ldots & \ldots & \ldots & .. \\ c_{N1} & c_{N2} & .. & c_{NN} & c_{NW} \\ 1 & 0 & 0 & -1 & 1 \end{bmatrix} \begin{bmatrix} \mu_1 \\ \mu_2 \\ .. \\ \mu_N \\ \mu_W \end{bmatrix} + \begin{bmatrix} b_{11} & b_{12} & \ldots & b_{1N} & 0 \\ b_{21} & b_{22} & \ldots & b_{2N} & 0 \\ \ldots & \ldots & \ldots & \ldots & .. \\ b_{N1} & b_{N2} & .. & b_{NN} & 0 \\ 0 & 0 & 0 & 0 & 0 \end{bmatrix} \begin{bmatrix} \sigma_1 \\ \sigma_2 \\ .. \\ \sigma_N \\ 0 \end{bmatrix} = 0 \qquad (14)$$

Eq. (14) can then be solved for the unknown doublet strengths μ_j.

3.2 Wake Relaxation and Discretized Wake Method

Inviscid flow characteristics perform a critical role in the calculation of the aerodynamic coefficients of lift, drag and moment. Subsequently, for the development of an effective and accurate aerodynamic model of a single- or multi-element airfoil, the complex interactions that occur between each element and their resultant downstream wake must be considered. In a single-pass panel method scheme, a fixed von Kármán wake panel of infinite length is attached to the airfoil's trailing edge and orientated to align with the trailing edge's bisector angle or the free-stream velocity. The wake induces an influence onto the airfoil and subsequently must be incorporated into the coefficient of pressure distribution across the element's surface [7].

Calculations of aerodynamic coefficients depend on the shape and orientation of the wake, which influences the Kutta condition. A single fixed wake oriented at the trailing edge bisector angle models the flow quite accurately near the trailing edge but fails to follow the flow field at larger distances downstream, therefore violating the conservation of momentum principle, overestimating lift and underestimating induced drag [11]. In addition, when the wake is oriented to align with the free-stream flow, it satisfies the conservation of momentum principle but fails to model the flow accurately along the

trailing edge [11]. The implementation of a single von Kármán wake panel for each element of multi-element airfoil model [7] has been demonstrated to fail when the distance between the elements is less than .005 times the chord length, causing the wakes to pass through the body of other elements and violating the boundary conditions.

To model the aerodynamic coefficients more accurately, the wake needs to be force-free and therefore oriented to align with the dominant local velocities; this is achieved through the implementation of a wake relaxation algorithm. Wake relaxation is accomplished by discretizing the wake profile through a series of sequential panels instead of as a single fixed panel. Each wake panel is aligned to the local velocity field, thereby satisfying the flow conditions both at the trailing edge and further downstream where the free-stream velocity is dominant and also maintaining the conservation of momentum principle [7].

To date, there are two methods commonly employed to derive wake profiles behind an airfoil, these are the time stepping scheme and spatial wake relaxation method [7-10]. Each method requires the wake to be discretized to enable the wake to deform.

Time-stepping wake relaxation is typically applied to simulations operating with unsteady motion [7-10]. In this procedure, the vorticity and flow field are calculated across the airfoil's profile as the wing moves forward with velocity Q_∞ at each time step Δt. The wake is shed from the trailing edge at each time step, maintaining the flow tangency [7]. Kelvin's circulation theorem, which states that the circulation around a closed body is constant with respect to time, is incorporated in addition to boundary conditions to maintain the total circulation around the airfoil and tangential flow [7].

The spatial wake relaxation method initializes the aerodynamic model with an arbitrary wake shape. The velocities of the wake panels are computed using this initial wake shape. Next, the wake panels are rotated to align with the local flow field giving a new wake shape. This procedure is repeated until a convergence criterion is satisfied [7].

The time-stepping wake relaxation technique is much faster than spatial wake relaxation since the wake panels increase at each time step, resulting in $NK/2$ number of iterations for N wake panels in K time steps [7]. However, as spatial wake relaxation has a predefined number of wake panels, the number of iterations is NK [7]. For multi-flap system, spatial wake relaxation converges in 2-3 iterations.

Spatial wake relaxation employs an iterative procedure to calculate the wake shape. Initially, an arbitrary wake shape is assumed that is shed along the free stream. The wake panels are oriented at the same angle and form a straight line being shed from the trailing edge. This initial configuration of airfoil and wake is solved to determine the source and doublet strengths on the airfoil, the pressure coefficients, and the wake geometry using a constant strength doublet-source panel method. The velocities induced on the wake panels by the new source and doublet strengths are calculated using a subroutine for each wake panel collocation point by the following equations [3]:

$$u_d = \frac{\mu}{2\pi}\left[\frac{z_i}{(x_i - x_j)^2 + z_i^2} - \frac{z_i}{(x_i - x_{j+1})^2 + z_i^2}\right] \tag{15}$$

$$w_d = \frac{-\mu}{2\pi}\left[\frac{x_i - x_j}{(x_i - x_j)^2 + z_i^2} - \frac{x_i - x_{j+1}}{(x_i - x_{j+1})^2 + z_i^2}\right] \tag{16}$$

$$u_s = \frac{\sigma}{4\pi}\left[\frac{(x_i - x_j)^2 + z_i^2}{(x_i - x_{j+1})^2 + z_i^2}\right] \tag{17}$$

$$w_s = \frac{\sigma}{2\pi}\left[\tan^{-1}\frac{z_i}{x_i - x_{j+1}} - \tan^{-1}\frac{z_i}{x_i - x_j}\right] \tag{18}$$

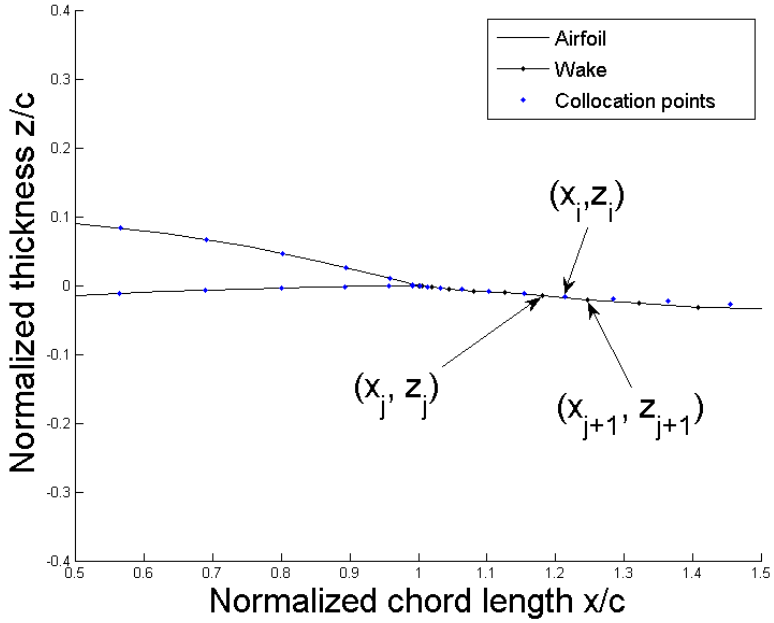

Figure 8: Discretized wake profile for wake relaxation

where (x_j, z_j) and (x_{j+1}, z_{j+1}) are panel end points, and (x_i, z_i) is a wake collocation point, in panel co-ordinates as shown in Fig. 8. The velocities (u_d, w_d) and (u_s, w_s) are induced by doublets and sources respectively and need to be converted into the global coordinate system using the inverse of the transformations given in Eq. (2). The summation of induced velocities in both x and z directions are then added to the free stream velocity components, and the resultant velocities are calculated.

The following equation given in [11] is used to calculate new x- and z- coordinates of the wake panel end points caused by the resultant velocity induced on the wake panel:

$$\frac{dz}{dx} = \frac{w + U_z}{u + U_x}$$

$$w = w_d - w_s \tag{19}$$

$$u = u_d - u_s$$

where u and w are the induced velocities on the wake panels, and U_x and U_z are the free stream velocities components.

The new positions of the wake panel end points are calculated by integrating Eq. (19). For example, by taking the end points of the first wake panel, which is located just aft of the trailing edge, the equation will yield its new orientation. Using the now-rotated first wake panel, the orientation of the second wake panel can be determined and so on. The following equation illustrates the procedure:

$$z_j = z_{j-1} + (x_j - x_{j-1}) \times \frac{w + U_z}{u + U_x} \tag{20}$$

$$x_j = x_{j-1} + (z_j - z_{j-1}) \times \frac{u + U_x}{w + U_z} \tag{21}$$

Here, the z coordinate of j^{th} panel end point is calculated using the induced velocities and coordinates of $(j\text{-}1)^{th}$ panel end point updated earlier in the loop. The x coordinate of j^{th} panel end point is then calculated by using updated value of z coordinate. The loop continues for all wake panel points.

Once the new wake profile is generated, new values of doublet strengths and pressure coefficients are calculated using a constant strength doublet panel method. The procedure is repeated until the wake shape is converged. The convergence criterion is the

assessment of the z-displacement of the wake end points between sequential iterations until a displacement of less than 0.001 is achieved. This value indicates that the change in the wake panel influence is insignificant when the change is z-displacement is small enough [7].

Figure 9 shows two simple wake assumptions and the results of the iterative procedure of wake relaxation for the NACA 4412 airfoil at an angle of attack of 15°. The wake consists of 50 wake panels with a half cosine distribution and a total length of 20 chord lengths. The length of the first wake panel is the same length as the trailing edge panel on the airfoil, and a Von-Kármán wake panel is added at the end of the wake. The von Kármán wake panel is added to prevent the wake panels towards the end from rolling up. For panels towards the end and away from the airfoil body, the influence of the airfoil reduces and there is no counter acting induced velocity in the opposite z-direction for these panels. Including a Von-Kármán wake panel of infinite length (~20 times chord length), solves this problem. The Von-Kármán wake panel is initially aligned along with other wake panels. When the wake is converged, the Von-Kármán wake panel orients itself parallel to the free stream.

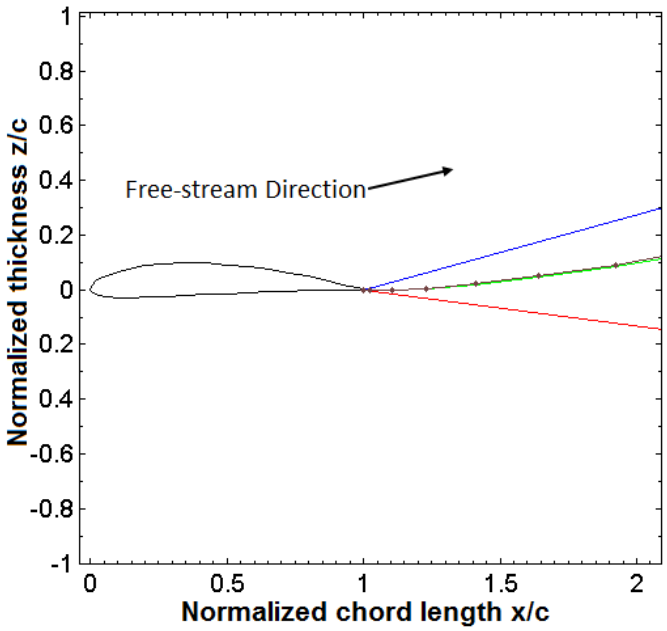

Figure 9: Wake profiles computed using different assumptions: free stream-aligned wake (blue), trailing edge bisector-aligned wake (red), and discretized wake panel relaxation scheme (green)

The panels near the trailing edge align to the trailing edge bisector, and panels away from the airfoil align with the free stream.

3.3 Three-Dimensional Panel Method

So far we have discussed the two dimensional panel method solution for a single airfoil. To extend this method into three dimensions, the VSAERO algorithm is used [11].

Let us consider the wing geometry in Fig. 9. Similar to the two-dimensional case, the wing geometry is discretized into an array of quadrilateral panels distributed across both the airfoil body and trailing edge wake. Constant-strength distributions of doublet singularities of unknown strengths are located on the four edges of each panel [6-10]. The doublet distribution enables the potential flow over the wing to be modeled such that

it satisfies the Neumann boundary layer condition, which states that the normal flow velocity across the wing's surface is zero [6-10]. This is mathematically represented by

$$\frac{\partial v_{surface}}{\partial n} = 0 \tag{22}$$

Using the Neumann boundary condition allows the modeling of thinner airfoils compared to the Dirichlet boundary condition, which is applicable for thick airfoils only. Since the flaps used in the MFS fall into the category of thin airfoils, Neumann is determined to be the most suitable boundary condition for this model.

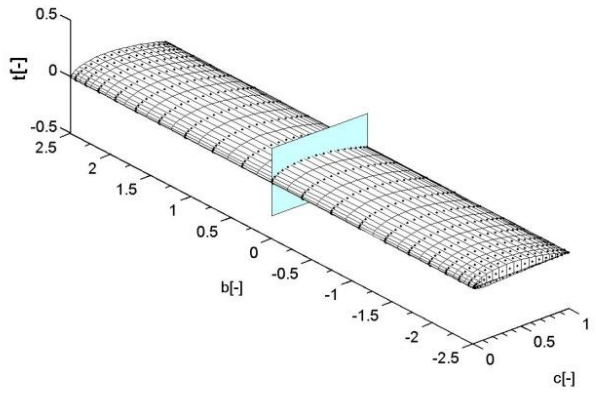

Figure 10: NACA 4412 wing geometry for validating the panel method, with an aspect ratio of 5. The cutting plane shows the mid-span section where C_p values are compared with two dimensional results.

The collocation points are assumed to be located at the centroid of the quadrilateral panels, and the doublets are situated on the quadrilateral panel edges with start and end points (x_1, y_1, z_1) and (x_2, y_2, z_2), respectively. These singularities induce a velocity on every collocation point (x_p, y_p, z_p) according to the following equations,

$$u = K(\mathrm{r}_1 \times r_2)_x\,,\ v = K(\mathrm{r}_1 \times r_2)_y\,,\ w = K(\mathrm{r}_1 \times r_2)_z \tag{23}$$

$$K = \frac{\mu}{4\pi \mid r_1 \times r_2 \mid^2}\left(\frac{r_0 \cdot r_1}{r_1} - \frac{r_0 \cdot r_2}{r_2}\right) \tag{24}$$

$$r_1 = (x_p - x_1)\hat{i} + (y_p - y_1)\hat{j} + (z_p - z_1)\hat{k},\ r_2 = (x_p - x_2)\hat{i} + (y_p - y_2)\hat{j} + (z_p - z_2)\hat{k},$$
$$r_0 = (x_2 - x_1)\hat{i} + (y_2 - y_1)\hat{j} + (z_2 - z_1)\hat{k} \tag{25}$$

The total induced velocity on each collocation point is the sum of the velocities induced by each edge of the quadrilateral panels on both the body and wake. To form a set of linear equations, the induced velocities are obtained on each collocation point by initially defining the doublet strength, μ=1, in Eq. (24). This provides the influence coefficients, which, when multiplied with the unknown doublet strengths, satisfy the Neumann boundary condition [6]. The resultant equation is given by

$$\sum_{k=1}^{N} C_{ik}\mu_k + \sum_{l=1}^{N_w} C_{il}\mu_l = -Q_\infty \cdot n_i \tag{26}$$

This equation is the discretized form of Eq. (22), where Q_∞ is the free-stream velocity and C_{ik}, C_{il} are the influence coefficients calculated by taking the dot product of the induced velocity on collocation point *i* by body panel *k* and wake panel *l* and the normal vector n_i of panel *i*. The unknown doublet strengths, μ_k and μ_l, are defined at the collocations points of body and wake panels. This equation satisfies the condition that the normal velocity on the wing surface is zero.

The Kutta condition is the same as in the two-dimensional case and is given by

$$\mu_{wake} = \mu_{upperTE} - \mu_{lowerTE} \tag{27}$$

where $\mu_{upperTE}$ is the doublet strength of the upper trailing edge panels and $\mu_{lowerTE}$ is the doublet strength of the lower trailing edge panels. This condition is incorporated by creating an augmented influence matrix *A*, where $A_{ik} = C_{ik}$ if no wake is shed from the body panel *k* (panel *k* is not a trailing edge panel), $A_{ik} = C_{ik} - C_{il}$ if the panel *k* is a lower trailing edge panel, and $A_{ik} = C_{ik} + C_{il}$ if the panel *k* is an upper trailing edge panel [6]. The resulting equation becomes

$$\sum_{k=1}^{N} A_{ik}\mu_k = -Q_\infty \cdot n_i \tag{28}$$

This system of linear equations is solved to obtain the unknown doublet strengths, which are then used to calculate the aerodynamic coefficients. The tangential surface velocity and coefficient of pressure at each collocation point is given by

$$\vec{V} = [u, v, w] + [U_\infty, V_\infty, W_\infty] - \frac{1}{2}\nabla\mu \tag{29}$$

$$C_p = 1 - \frac{|V|}{|Q_\infty|} \tag{30}$$

$$Q_\infty = [U_\infty, V_\infty, W_\infty] \tag{31}$$

where the $[u, v, w]$ velocity components are calculated using Eqs. (29), (30) and (31) and $[U_\infty, V_\infty, W_\infty]$ are the components of the free-stream velocity. The induced velocity on wake panels is also calculated to apply wake relaxation.

3.4 Unsteady Panel Methods

The VSAERO panel method algorithm requires a user-defined initial wake geometry that can be tedious for multi-element airfoils due to the number of potential permutations

for a morphing wing geometry. For example, the flap configuration presented in Fig. 10(a) employs a wake geometry that is oriented to align with the free-stream velocity and incurs no interaction with elements located downstream. However, if the same technique is applied to the flaps when in the rest configuration, as seen in Fig. 10(b), the wake shed from the leading edge intersects the body of trailing edge flap, violating the non-permeability boundary condition over the surface of the body.

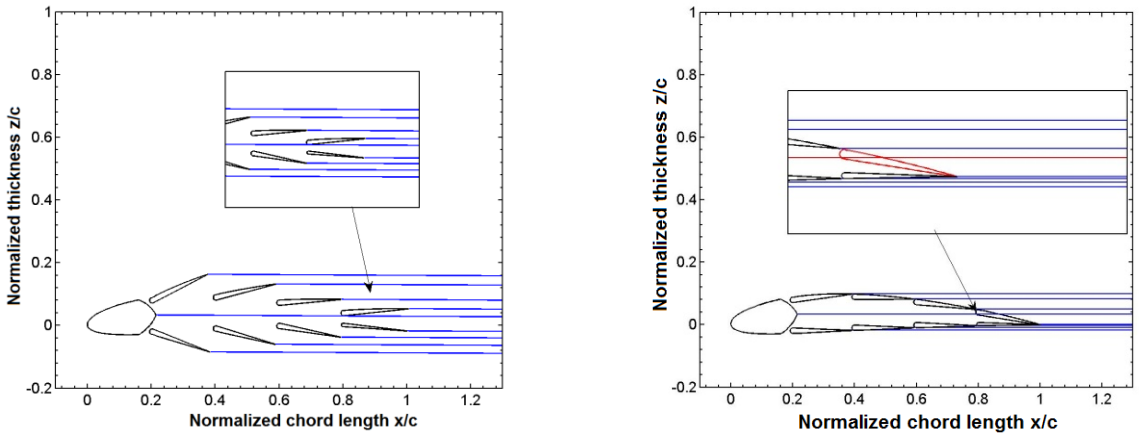

Figure 11: When using a user-defined wake, a standard wake shape is not suitable for all the flap configurations.

Unsteady panel methods offer the advantage of resolving wake shapes during each iteration, thereby eliminating the user's trial and error to define a suitable wake profile for each flap configuration. The orientation of each flap is calculated, and a buffer wake panel is attached to each trailing edge, shown in Fig. 11. As the solution advances with each time step, wake panels are added and aligned along the direction of local velocity [7, 11, 12]. For unsteady flow scenarios such as a gusting flow, the solution is advanced until the final time of the simulation; whereas, in steady state problems, the solution iterates until a steady state wake profile is achieved. During previous studies, a steady state wake

is achieved at 20 chord lengths aft of the airfoil's trailing edge; beyond this point the turbulence within the wake is assumed to have dispersed [7].

The initial geometry of body and buffer wake panels shown in Fig. 11 is solved using a constant-strength doublet panel method as discussed in the previous sections. The kutta condition is applied on the buffer wake panels and the unknown doublet strengths are calculated.

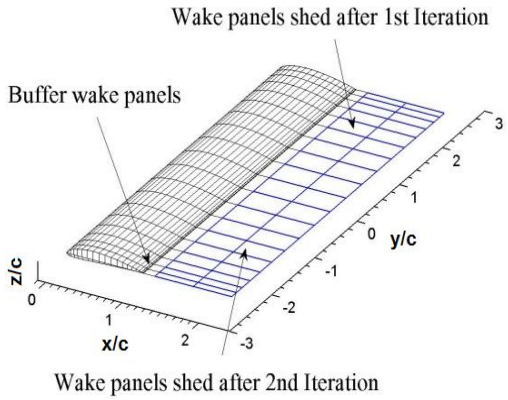

Figure 12: Initial Geometry for unsteady panel method with buffer wake panel

After calculating the doublet strengths for this configuration, the time step is advanced by Δt defined by

$$\Delta t = \frac{t}{N_t} \tag{32}$$

where t is the total time of simulation. For steady cases, the simulation is stopped when wake length becomes 20c and thus t is calculated by dividing this wake length by the free-stream velocity. N_t is the number of wake panels, which depend on the length of the trailing edge panel [4-7]. The first wake panel is then installed downstream of the buffer wake panel. The doublet strength of this wake panel is set equal to strength of the buffer panel from the previous time step [7]. Subsequently, the right-hand side of Eq 28 is

updated to include the influence of the new wake panel, and the linear system is solved again to obtain the doublet strengths on the body and buffer wake panel. Each subsequent wake panel is added between the buffer wake panel and the wake panel of the previous iteration, which is advanced by the distance $V\Delta t$, where V is the induced velocity on the wake panel, to model its convection downstream. As discussed earlier, this process is repeated until the wake length is equal to 20 chord lengths. At distances further than this, the velocity induced by a body panel, which is inversely proportional to the distance from the panel, becomes negligible, and the wake merges with the free stream. The induced velocities incurred by the wake collocation points are calculated using Eqs. (29-31). Further details on unsteady panel methods and its implementation for multi-elements wings can be found in [6].

An important flow phenomenon that requires consideration is the wake roll up occurring aft of the wing tips. The roll up is caused by the span-wise vorticity gradient and is generated as a part of the solution when wakes are shed along the local free-stream velocity. Figure 12 shows the wake roll-up behind a NACA 4412 [20, 21, 23].

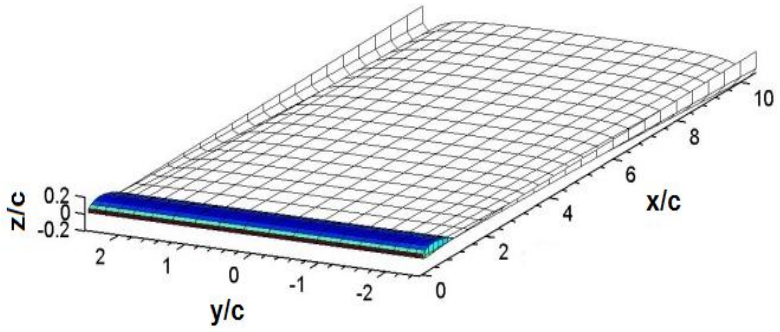

Figure 13: Wake roll up and C_p distribution achieved at the steady state for NACA 4412 wing with an aspect ratio of 5 and $\alpha = 0^\circ$.

3.5 Vortex Particle Method

Using a discretized wake with an unsteady panel method is more robust than methods employing user-defined wakes. However, this method has disadvantages with respect to wake panel lengths. For certain flap configurations where two elements are very close to each other (~0.002c), large wake panels (greater than the spacing between the elements) fail to maintain the integrity of the boundary condition, which can be seen in Fig. 13. Once the boundary condition is violated, the solution generates wake profiles which are physically impossible. To overcome this issue, wake panels near any of the airfoil's elements need to be redistributed so that their length is less than the gap between the elements. This process involves identifying such cases in each iteration and redistributing the velocities over new wake geometry using the calculated velocities from the previous one. However, implementing this method in three dimensions with complex geometries is tedious and increases computation time.

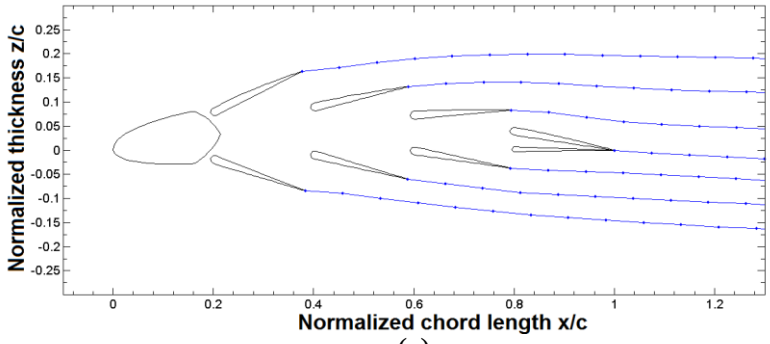

(a)

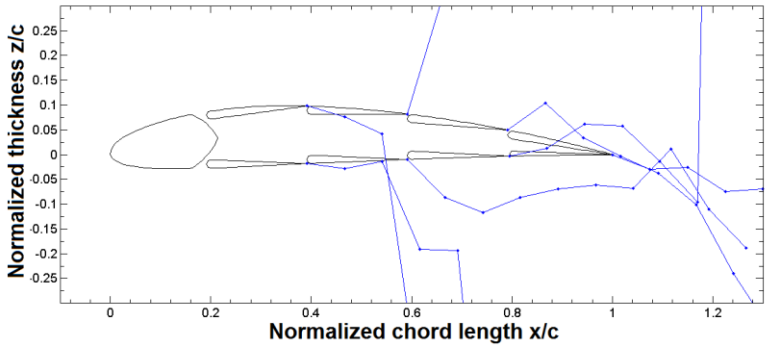

(b)

Figure 14: (a) Discretized wakes shed from trailing edge of flaps following the local velocity vectors when the distances between flaps are comparable to wake panel lengths. (b) Wakes violating non permeability boundary condition when distance between sequential flaps is smaller in comparison to wake panel lengths.

An alternative way is to represent wakes as vortex particles, also known as vortrons. In this method, the wing and the buffer wake geometry are solved using a traditional panel method discussed in Section 3.3, but instead of shedding wake panels, the doublet sheets of buffer wake panels are collapsed into vortex particles and shed into the fluid domain [16-19].

Vortrons are singularities defined by a strength vector and a position vector [16]. The position and strength of each vortron is dependent on the vorticity added into the domain in each iteration and is governed by transport Eqs. (33-34) [16]

$$\frac{d}{dt}\vec{R}_p(t) = \vec{U}_p\left(\vec{R}(t),t\right) \tag{33}$$

$$\frac{D\vec{\alpha}_p(t)}{Dt} = \vec{\alpha}_p(t)\cdot\nabla\vec{U}_p\left(\vec{R}(t),t\right) \tag{34}$$

where $\vec{R}_p(t)$ represents the position vector of the vortex particle, $\vec{\alpha}_p(t)$ is the strength vector, and $\vec{U}_p\left(\vec{R}(t),t\right)$ is the induced velocity on each particle. The induced velocity on a vortex particle is the summation of all the induced velocities by wing and buffer wake panels and other vortex particles. The induced velocity by the wing and buffer wake

geometry is calculated using Eqs. (23-25), and the induced velocity by all vortex particles at a point $\vec{R}$ is given by [16]

$$\vec{U}_p(\vec{R}(t),t) = \frac{1}{4\pi}\sum_p \nabla\left(\nabla\frac{1}{\left\|\vec{R}-\vec{R}_p(t)\right\|}\times\vec{\alpha}(\vec{R},t)\right) \tag{35}$$

Discretized forms of Eqs. (34-36) are available in [17].

In each iteration, the buffer wake doublet panels are first converted into vortex sheets to calculate the equivalent circulation. This procedure is simple for quadrilateral doublet panels because mathematically it is equivalent to a vortex sheet [7]. Thus, the circulation is equal to the doublet strength. Next, the number of vortex particles to be shed from each vortex sheet is chosen, and the vortex sheet is divided into equivalent segments [17]. The initial position of the vortex particle is assumed to be at the centroid of each segment, and its strength is calculated by multiplying the change in circulation with the area represented by the segment. This formula is derived from Kelvin's circulation theorem [17]:

$$\left[\frac{d\Gamma}{dt}\right]_{wing} = -\left[\frac{d\Gamma}{dt}\right]_{wake} \tag{36}$$

Once the particles are shed into the domain, they are governed by the transport equations and thus are not confined to the geometry constraints imposed on discretized wake panels [16]. The velocity induced by vortex particles on the wing is included in the RHS of Eq. (28) for each iteration, and the process is governed by the same steady-state stopping condition as in the case of an unsteady panel method.

Figure 14 shows the wake represented by vortex particles in single and multi-element wings.

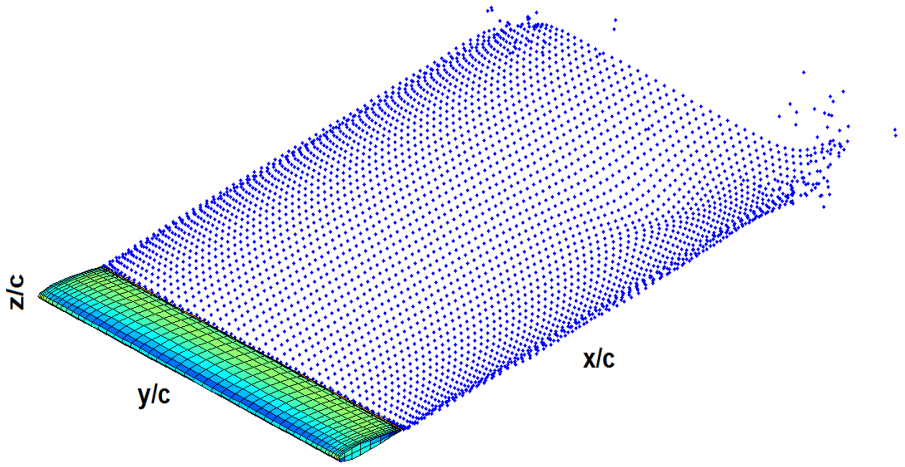

(a)

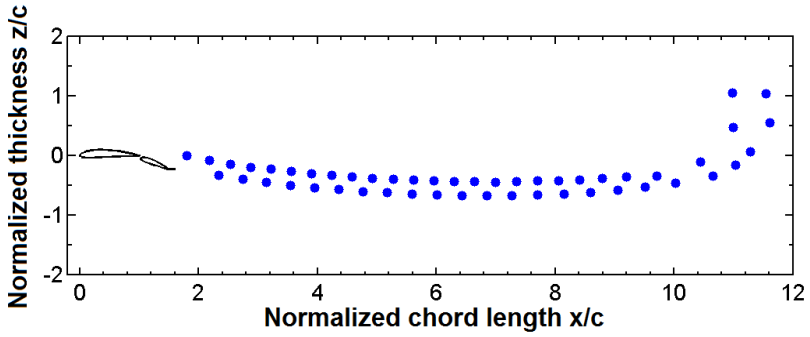

(b)

Figure 15: (a) Vortex particle wake shed behind a NACA 0012 wing with an aspect ratio of 5 and α=5°. (b) Wake roll behind two-element airfoil using vortex particles (Wing- NACA 4412, Flap- NACA 4415), α=0°.

3.6 Viscous Formulation

The implementation of an unsteady panel method enables the inviscid flow characteristics, tangential surface velocity u_e, and coefficient of pressure C_p, to be calculated. However, to create an accurate representation of the fluid flow around the vehicle, a viscous flow model must be incorporated. Both the inviscid and viscous flow components are critical in calculating an accurate result for lift, drag and moment

coefficients, especially at higher angles of attack where sensitivity to flow separation and stalling increases.

For the development of this multi-element model, a one-equation boundary layer scheme is employed across the airfoil surface and the laminar, transition, turbulent and separated flow regimes are determined sequentially. Initially, the tangential surface velocity for each element is assessed for a stagnation point, where $u_e = 0$, near the leading edge. The location of this point is dependent on the inbound free-stream velocity, angle of attack, and the flap configuration employed and defines where an inbound streamline, or the wake from another airfoil, interacts with the airfoil surface, thereby driving the fluid flow to diverge around the airfoil's upper and lower surfaces. However, due to the complexity of the fluid flow around a multi-element airfoil, the elements are assessed from forward to aft, rather than simultaneously, as the potential of flow separation, due to a turbulent regime, would alter the location of wake reattachment to elements further downstream. To model the viscous flow across the airfoil, each element is divided into an upper and lower surface relative to the stagnation point, and the boundary layer characteristics are calculated in terms of arc length, s, relative to this point.

Initially, each surface is assumed to be in the laminar regime immediately downstream of the stagnation point, where Thwaites method [7] is employed to model the growth of the momentum thickness, θ, and the dimensionless pressure gradient, λ, until flow transition, by Michel's criterion, Eq. 37, or separation, when $\lambda(s) \leq -0.09$ [7] ensues:

$$\mathrm{Re}_\theta > 1.174\left(1+\frac{22400}{\mathrm{Re}_s}\right)\mathrm{Re}_s^{0.46} \tag{37}$$

where, $\mathrm{Re}_s = \rho u_e s/\mu$ and $\mathrm{Re}_\theta = \rho u_e \theta/\mu$ are the arc length-dependent and momentum thickness-dependent Reynolds numbers, respectively.

During the transition region, instabilities exist within the flow and subsequently, for modeling purposes, the boundary layer is assumed to change instantaneously to the turbulent regime downstream of the transition point. The turbulent flow is modeled using Head's entrainment velocity method and continues to grow until either the flow separates, when $H(s) \geq 2.4$, relaminarization is achieved due to adverse pressure, or the airfoil's trailing edge is reached. The turbulent boundary layer requires the von Kármán momentum integral equation, Ludwieg-Tillman's skin friction law, and Cebeci and Bradshaw's empirical laminar and turbulent shape factor relationships to be solved simultaneously to calculate the momentum thickness θ, shape factors H and H^*, and coefficient of friction c_f. As the transition point is reached, the fluid characteristics at the transition point act as the initial values to continue these boundary layer parameters through the turbulent flow. For an in-depth review of this boundary layer model, please refer to Blower, Dhruv and Wickenheiser [4].

For situations where a forward element's wake interacts with an element downstream, the boundary layer is assumed to continue across the two elements. However, due to the Goldstein singularity, the one-equation boundary layer theory cannot be solved beyond flow separation[7]. To resolve this limitation, as the trailing edge wake is shear free the boundary layer is modeled as a Couette flow and any element surfaces within the resultant plum resume the forward element's boundary layer condition.

Upon completion of the boundary layer model across the entire airfoil, the coefficients of lift, drag and moment can be calculated across the airfoils' surfaces through the integration of the pressure and wall shear stress, $\tau_w = \frac{1}{2} c_f \rho u_e^2$.

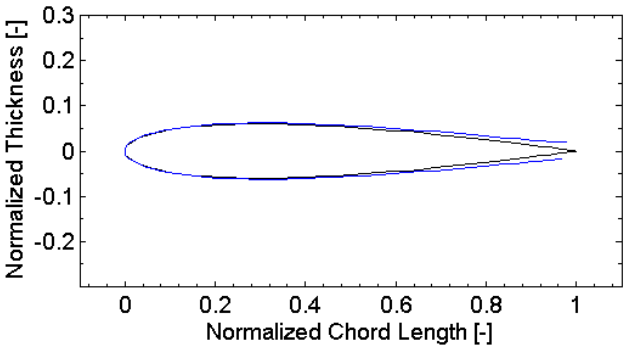

Figure 16. Boundary layer over a NACA 0012 airfoil at Re = 2000

Chapter 4- Results

4.1 Validation

Performing detailed error analysis on the results obtained from the methods discussed in the previous section provide a great insight into the characteristics of the flow over the airfoils and the fidelity of the method itself. For example, calculating the pressure distribution over a NACA 4412 wing using a doublet source panel method with different wake orientations show that the results are closer to the experimental [21] values when the wake is aligned to the local velocity vector. On the other hand, a wake parallel to the free-stream does not model the flow around trailing edge as accurately. This is because the wake orientation in this region should be along the trailing edge bisector angle. Further, if the wake in only aligned to the trailing edge bisector angle, even at distances far away from the airfoil, the conservation of momentum is violated. This results in over-estimation of the lift, as shown in Fig 17. The Root Mean Squared (RMS) error between the experimental and numerical results using a discretized wake is given by.

$$RMS_{error} = \sqrt{\frac{\sum_{i=1}^{N}\left[(C_p)_{\exp} - (C_p)_{numerical}\right]_i^2}{N}} \tag{39}$$

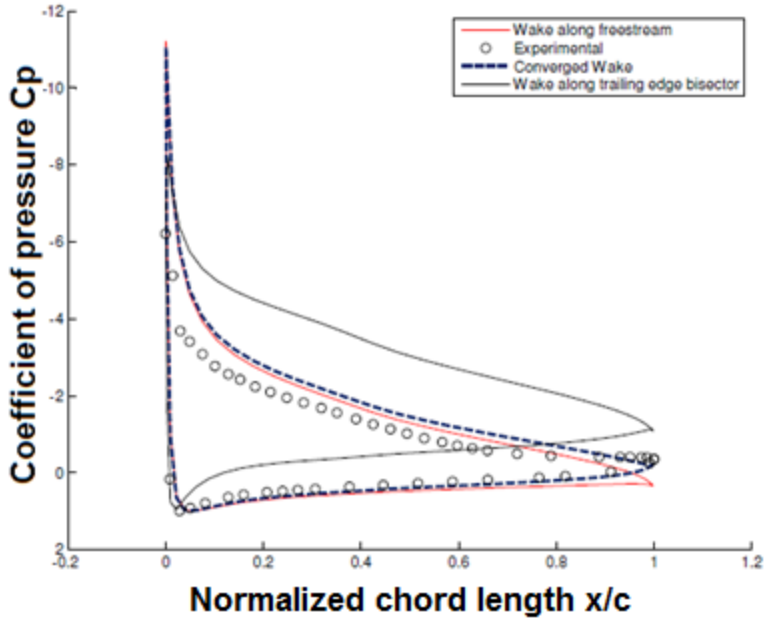

Figure 17: Coefficient of Pressure comparison for different wake profiles for NACA 4412 at angle of attack 13.87^{o}

This error is equal to 1.06 for a two dimensional doublet source panel method using a discretized wake.

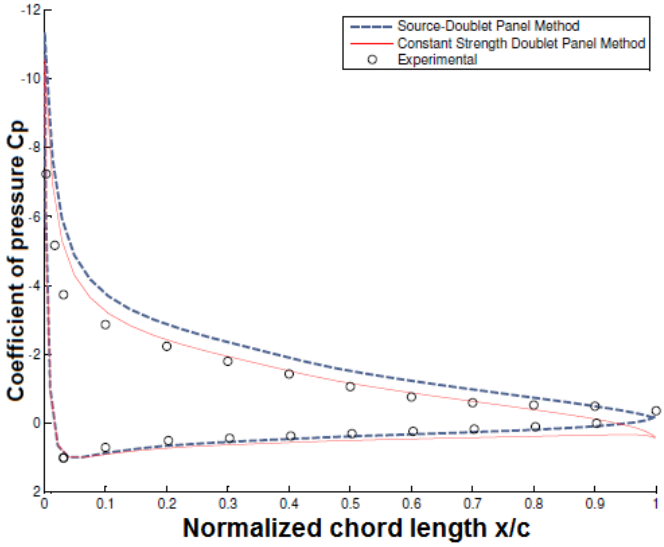

Figure 18: Coefficient of Pressure comparison obtained by different methods for NACA 4412 at angle of attack 13.87^{o}

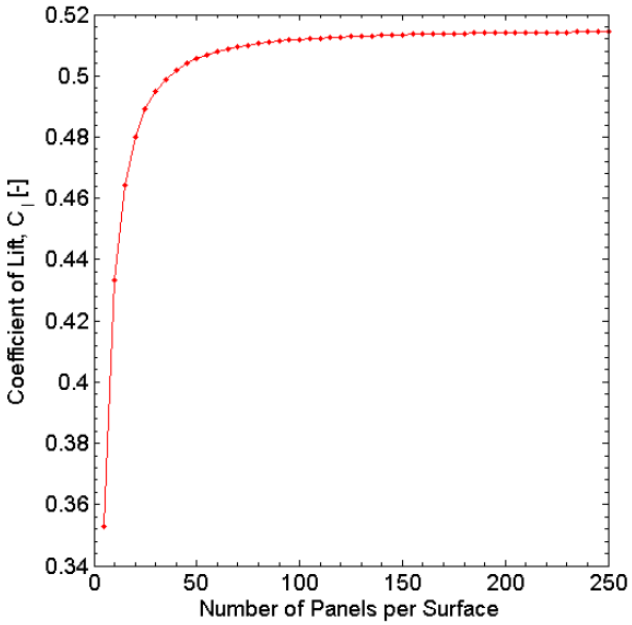

Figure 19: Variation of coefficient lift with respect to the panel density using a doublet source panel method over a NACA 4412 airfoil, angle of attack 0^o

The RMS error for a constant strength doublet panel method is 0.8171. Although the RMS error is relatively small in comparison to the doublet-source panel method, the viscous effects induced by the sources in the latter model the flow around the trailing edge quite accurately, as shown in Fig. 18. The increase in panel density representing the surface of the airfoil results in more accurate calculation of aerodynamic coefficients. For example, for a NACA 4412 airfoil with a unit chord length, convergence is achieved when more than 60 panels are used to represent its surface. Fig. 19 shows the variation in coefficient of lift as a function of number of panels at $\alpha=0°$.

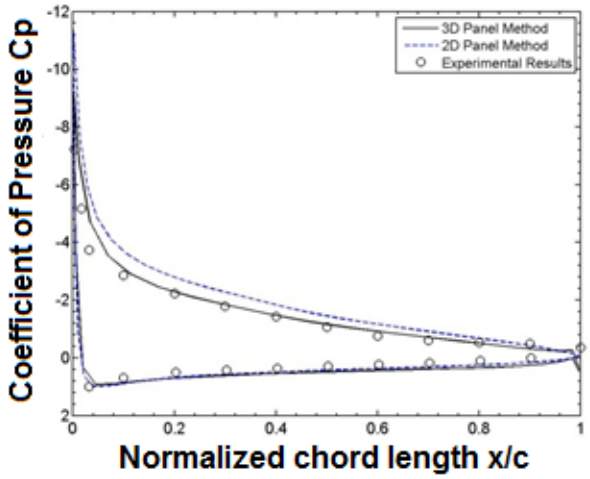

Figure 20: Validation of a single element 3D panel method in comparison to 2D panel method and experimental results [11, 12]. Aspect Ratio = 100, number of chord-wise panels = 40 and span-wise panels = 100,α=13.87°

The three-dimensional panel method is found to be nearly twice as accurate as the two-dimensional panel method with an RMS error of 0.5614 as shown in Fig. 20. This is because in three dimensions the span-wise vorticity gradient induces a downwash at the tips, which influences the pressure distribution at the mid-span location by decreasing the circulation. For higher aspect ratio wings, the influence of these vorticity gradients at the mid-span location is negligible, which causes the results to line up with two-dimensional experimental values. Thus, the three-dimensional analysis for higher aspect ratio wings provides more realistic results for two-dimensional experimental flows.

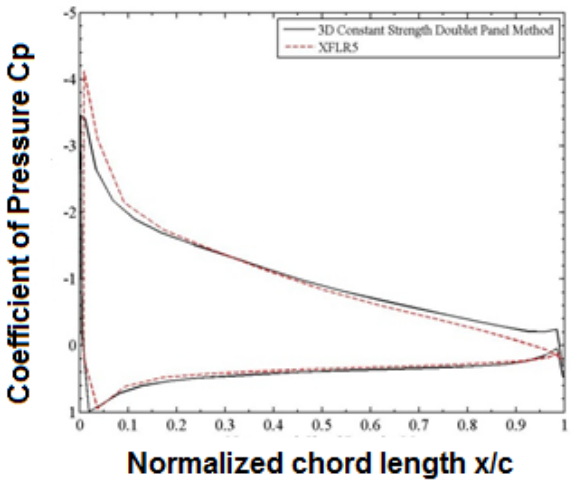

Figure 21: Validation of 3D panel method with XFLR5 for a NACA 4412 wing with an aspect ratio of 10, α=10, number of chord-wise panels = 40 and span-wise panels = 100,

The three-dimensional panel method when compared to the commercially available panel method solvers like XFLR5 show agreement with the results, as shown in Fig 21. The accuracy can be further increased by increasing the panel density over the surface of the wing.

The single-element panel method can easily be extended into a multi-element method by including influences of all the body and wake panels on a given collocation point and satisfying the Kutta condition for each element [4-9]. Fig. 22 shows a two-element wing, which when analyzed using a three-dimensional panel method, follows the predicted trend.

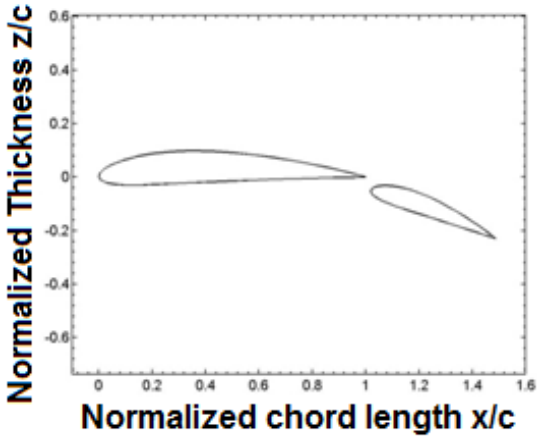

Figure 22: Two Element Airfoil (Wing NACA-4412 c=1.0) (Flap NACA-4415 c=0.5, deflection=21°

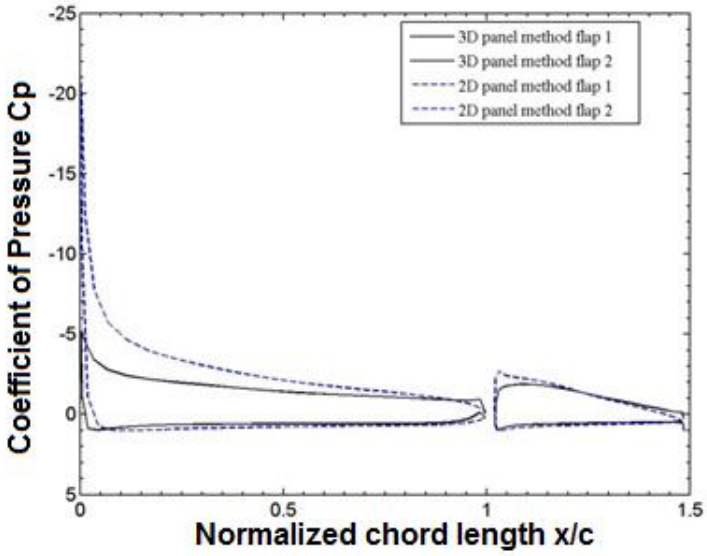

(a)

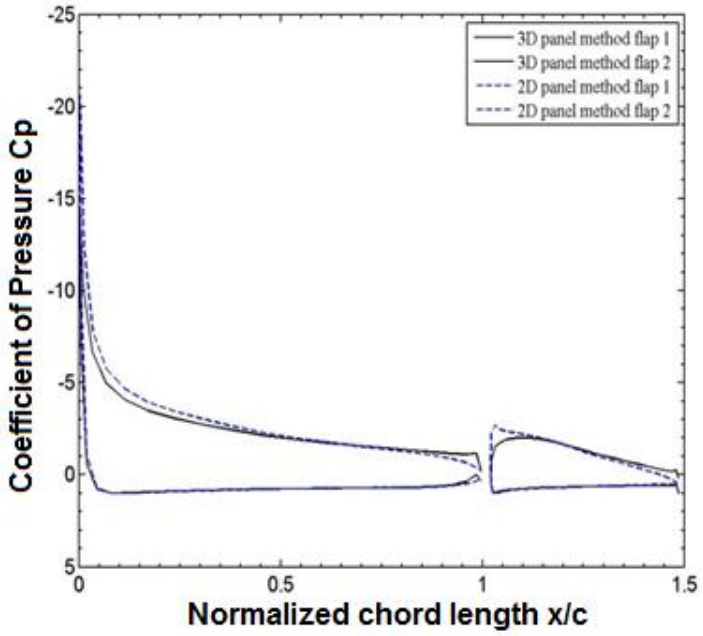

(b)

Figure 23: Comparison of 2D and 3D panel method (a) at aspect ratio = 5 (b) at aspect ratio = 20 and α=8.2°, showing how high aspect ratio wings behave like a 2D airfoil

At lower aspect ratios, the influence of span-wise vorticity gradients decreases the circulation at the mid-span location by inducing downwash [9, 10, 23], and hence the pressure gradient at over the surface of the wing is considerably less than the two-dimensional case, with an RMS error of 1.1. This comparison is shown in Fig. 23(a). However, with an increase in aspect ratio, the three-dimensional results align more closely to the two-dimensional calculations, validating the multi-element aerodynamic solver, as shown in Fig. 23(b).

The unsteady panel method shows a very distinct increase in circulation over the surface of the airfoil as time progresses. At each iteration, wake panels are added; this increase in wake length is marked by an increase in pressure distribution over the wing after each step, shown in Fig. 24(a). This occurs because the wake influence becomes stronger, increasing the values in the RHS of the linear system in Eq. (28).

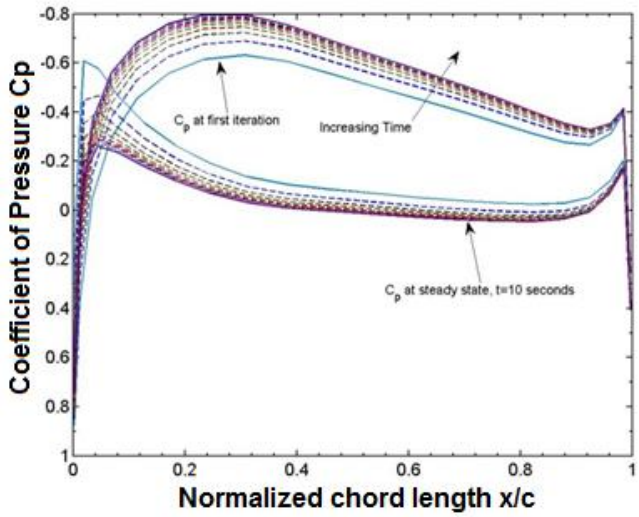

(a)

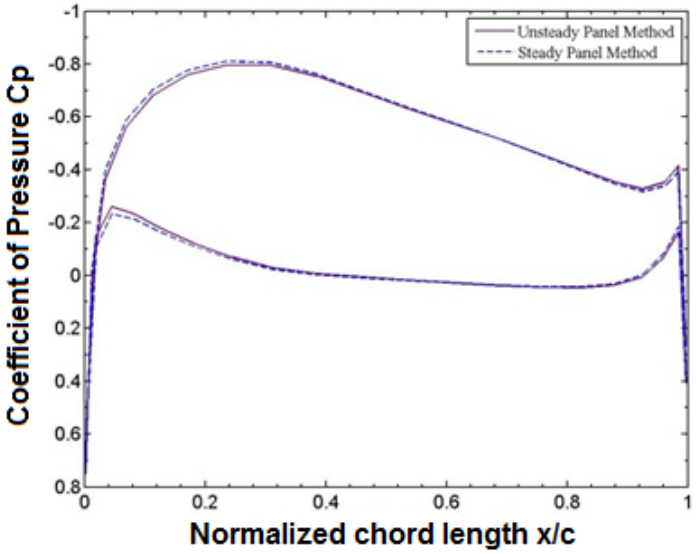

(b)

Figure 24: (a) Coefficient of Pressure at the midsection of a NACA 4412 wing with aspect ratio of 5 at α=0° at different time steps. (b) Comparison of the results of unsteady 3D panel method obtained at the steady state with that of the steady 3D panel method for a NACA 4412 wing with an aspect ratio of 5 at α=0°.

When steady state is reached, the pressure distribution over the surface is almost equal to the pressure distribution obtained using a steady panel method, as shown in Fig. 24(b). The RMS error between the two sets of values is 0.0178.

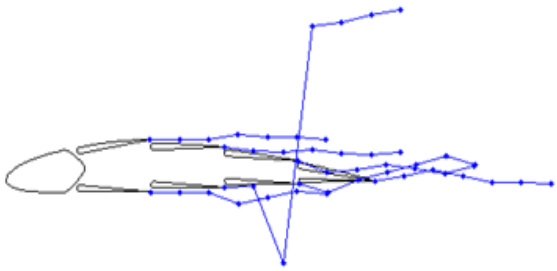

(a)

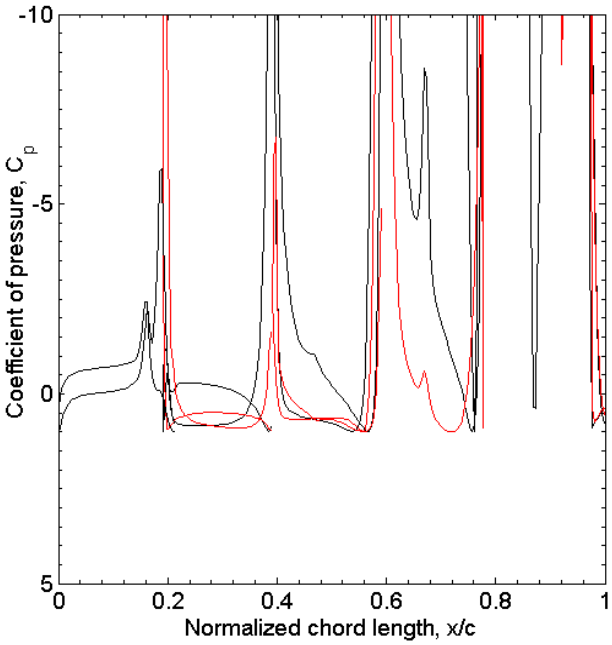

(b)

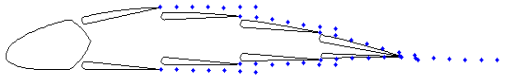

(c)

Figure 25: (a) Discretized wake method fails when flap distance are lesser than the wake panel lengths. (b) An unrealistic pressure profile is obtained when the wakes pass through the body of the flaps. (c) The vortex particle method resolves wake profiles for configurations when flap distances are less than ~.002c, resulting in accurate assessment of the aerodynamic coefficients.

Using a vortex particle method to represent the wake geometry in an unsteady panel method enables the user to model the aerodynamic behavior of flap configurations where the discretized wake method fails. When the flaps distance are in the range of .002c, for

example, the rest configuration of the MFS as shown in Fig. 25, using a discretized wake method causes the wakes to pass through body of the flaps resulting in unrealistic pressure profiles. For the same configuration, the vortex particle method accurately models the wake profile and thus enables the user to calculate the aerodynamic coefficients with ease.

Though the use of a vortex particle method results in less decision-making for the user, it is more computationally expensive. This is because the vortex-wake representation requires more than one particle per equivalent wake panel to obtain accurate results.

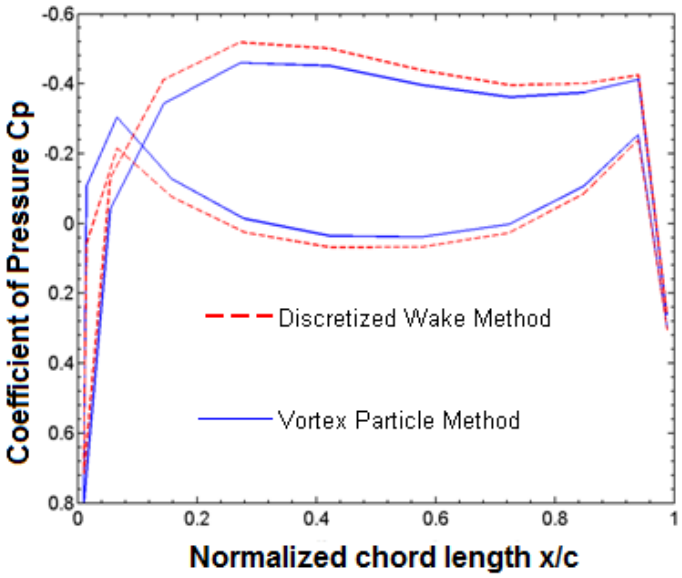

Figure 26: Comparison of coefficient of pressure C_p obtained by a vortex particle method and unsteady panel method (each wake panel is represented by two vortex particles).

When compared to results obtained from an unsteady panel method, plotted in Fig. 26, the RMS error between the vortex particle method and the unsteady panel method is 0.3329.

There is always a computational trade-off between choosing which method to employ. Generally speaking, the unsteady panel method can be used to analyze flap configurations where there is less possibility of strong wake-body interactions, and a vortex particle method is more suitable for configurations where sequential flaps are too close to each other (~.002c).

4.2 Aerodynamic Behavior of the Multi-Flap System

After the comparisons to existing methods in the 2D case, the viscous-inviscid method is applied to the three-dimensional analysis of the bio-inspired multi-flap system.

The idea of this system is to replace the traditional control surfaces and improve the aerodynamic capability of the aircraft. Thus, during cruise flight, when all flaps are in the rest configuration, the MFS should behave as a standard NACA airfoil.

Consider the MFS configuration with two independent flaps stations as shown in Fig. 27(a). The flaps at both stations are at rest configuration and thus mimic a NACA 4412 airfoil. Calculating the aerodynamic coefficient at the mid-span location of each flap configuration and comparing it with a NACA 4412 wing in Fig. 27(b) shows that the MFS can behave as a standard airfoil in cruise condition. For example, the coefficient of pressure C_p over the internal surfaces is nearly equal to 1; this means that there is no flow inside the body of the wing, thus preserving the integrity of the NACA 4412. The pressure spikes are due to the slot flow between the flaps which do not significantly affect the total lift generated over the surface of the wing.

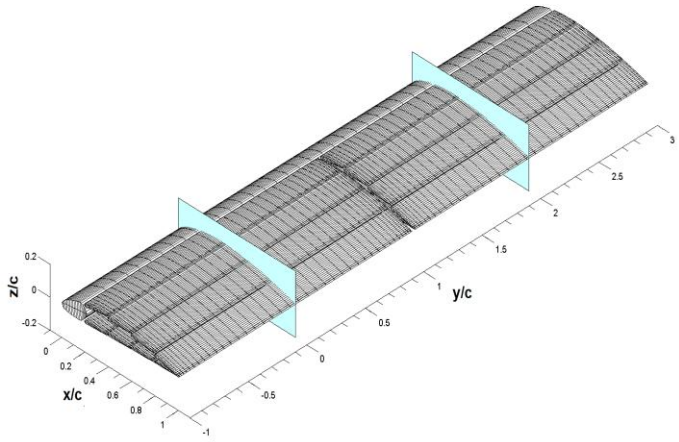

(a)

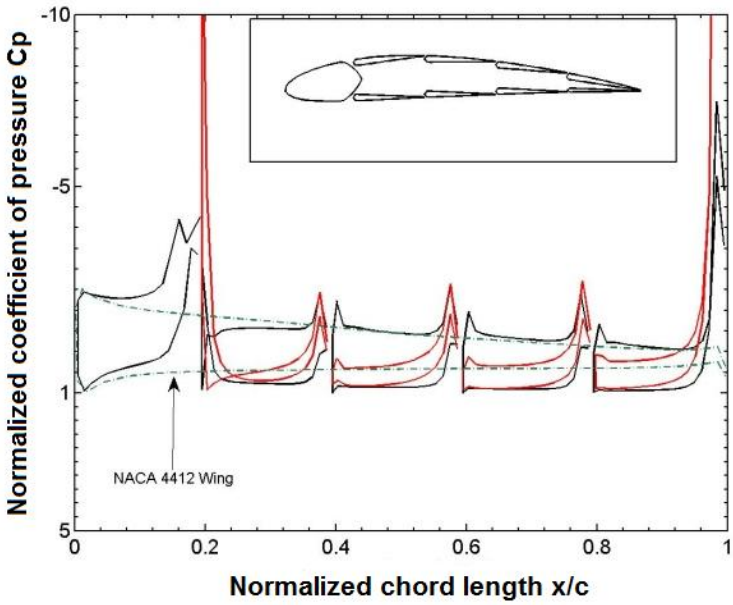

(b)

Figure 27: (a) Bio-inspired multi-flap system geometry with two span-wise systems of flaps (station 1 and station 2) where C_p is calculated at the mid-span sections for aspect ratio=4 with all flap deflections set to 0°. (b) Coefficient of pressure plots at mid-span sections for both station 1 and 2 (black upper flaps and leading edge, red-lower flaps, green- NACA 4412), α=10°, aspect ratio=4.

For the Multi-Flap System to replace traditional control surfaces, substantial claims should be verified that traditional aerodynamic motions can be produced by just using the MFS. Figure 28 shows a three-station MFS wing with pressure distributions over each section.

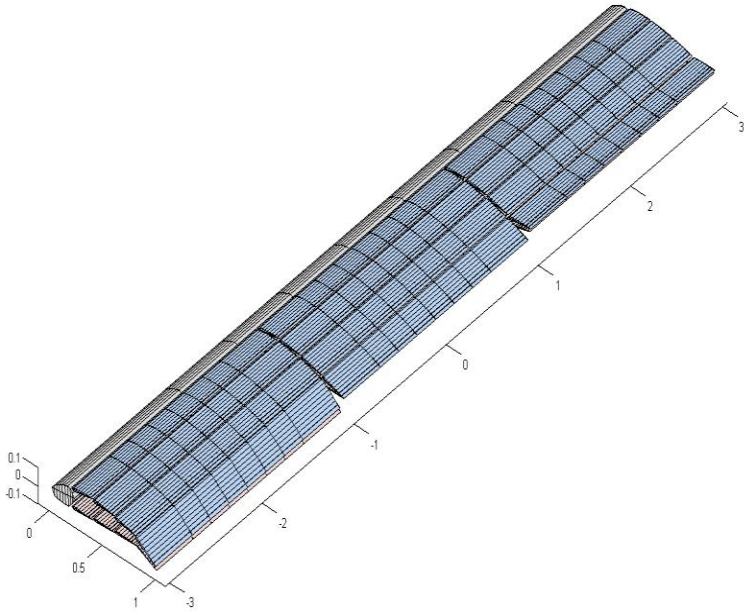

(a)

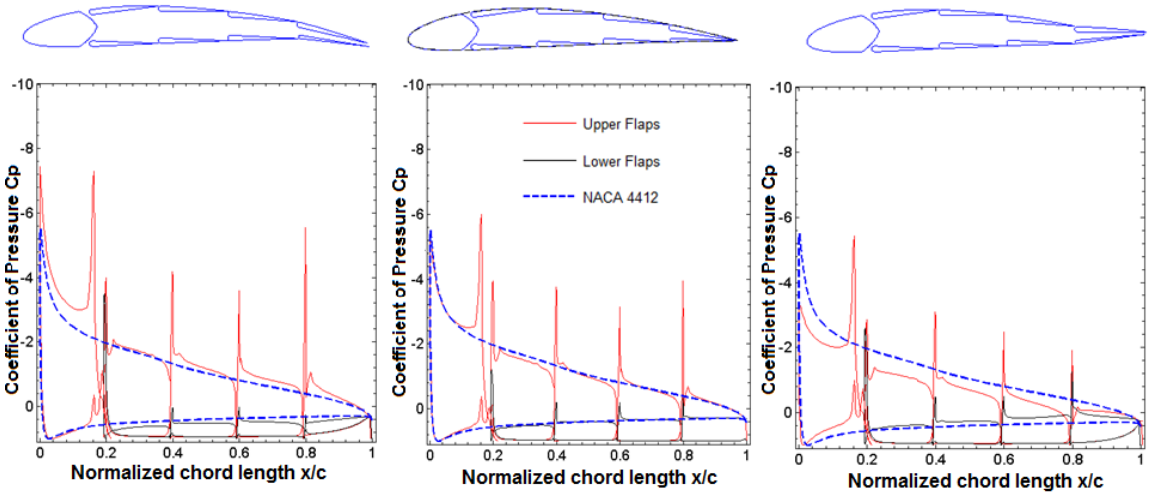

(b)

Figure 28: (a) Bio-inspired multi-flap system geometry with three span-wise systems of flaps and aspect ratio=6 with deflections

$$\delta_{11} = 0°, \delta_{12} = 0°, \delta_{13} = 0°, \delta_{14} = -5°, \delta_{15} = 0°, \delta_{16} = 0°, \delta_{17} = 0°, \delta_{18} = -8°$$
$$\delta_{21} = 0°, \delta_{22} = 0°, \delta_{23} = 0°, \delta_{24} = 0°, \delta_{25} = 0°, \delta_{26} = 0°, \delta_{27} = 0°, \delta_{28} = 0°$$
$$\delta_{31} = 0°, \delta_{32} = 0°, \delta_{33} = 0°, \delta_{34} = 9°, \delta_{35} = 0°, \delta_{36} = 0°, \delta_{37} = 0°, \delta_{38} = 7°$$

(b) Coefficient of pressure plots at mid-span positions for all the three stations α=10°, aspect ratio=6.

It can be observed that when the trailing edge flaps are deflected by a negative angle, there is a slight increase in the overall lift. Consequently, when the flaps are deflected by a positive angle, the lift decreases. Figure 28(b) shows an increase and a decrease in

pressure gradient along the span at different stations as a result of flap deflections. This simulates a roll motion on the aircraft as traditionally produced by asymmetric aileron deflections.

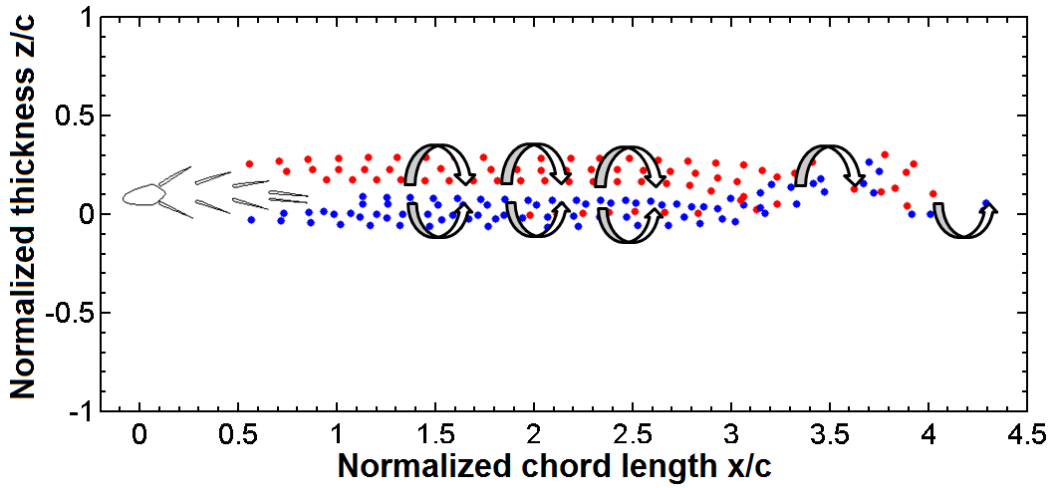

Figure 29: Vortex particle wake behind multi-flap system configuration for air braking, α=0°, $\delta_{11}=25°, \delta_{12}=20°, \delta_{13}=15°, \delta_{14}=5°, \delta_{15}=-25°, \delta_{16}=-20°, \delta_{17}=-15°, \delta_{18}=5°$

Interesting aerodynamic characteristics are obtained when analyzing different flap configurations. These aerodynamic characteristics contribute towards a range of complex maneuvers without compromising the stability of the aircraft. When all flaps are deflected outwards into the incoming flow, as depicted in Fig. 29, counter-rotating vortices are generated from their trailing edges. These vortices contribute to the form drag, resulting in air-braking. For a three-station wing like in Fig. 28(a), using this configuration on either station 1 or 3 while keeping the other stations in the rest configuration can induced rapid air-braking on one side resulting in a sharp yaw motion. This kind of maneuver can be used while negotiating around buildings in urban environments.

When encountering gusts at higher angles of attack, separation is a major concern for UAVs using traditional control surfaces. Separation results in loss of lift, making it impossible to control the aircraft and potentially leading to damages or loss. On the other hand, while using the MFS, a slight deflection of flaps along the direction of the flow as shown in Fig. 30 induces high pressure gradients on the surface of each flap that can resist the adverse pressure gradient reattaching the separated flow.

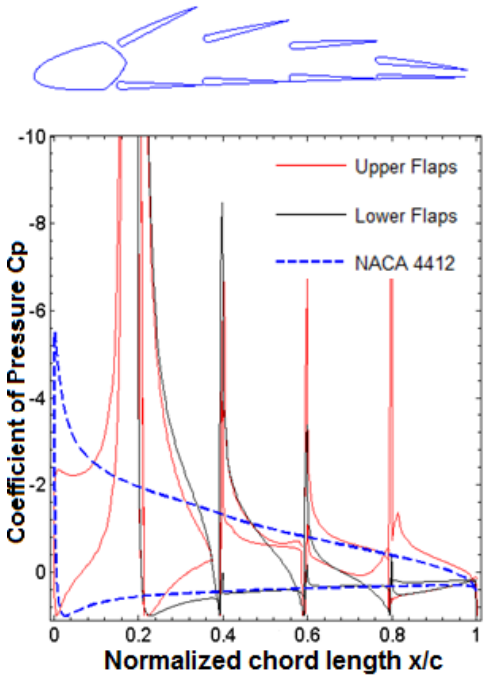

Figure 30: Bio-Inspired Multi-Flap Configuration to delay separation and avoid gust, α=10°, $\delta_{11} = 5°, \delta_{12} = 4°, \delta_{13} = 3°, \delta_{14} = 1°, \delta_{15} = 0°, \delta_{16} = 0°, \delta_{17} = 0°, \delta_{18} = 0°$

The MFS thus generates both traditional and no-traditional aerodynamic motions, enhancing the ability of the complete system. A MFS wing using three flap stations models a wide range of basic and complex aerodynamic maneuvers. For example, the configuration in Fig. 31 can be used in cruise flight where steady lift is desired. To generate a roll motion, the trailing edge flaps at station 1 and 3 are deflected in opposite direction as shown in Figs. 32 and 33.

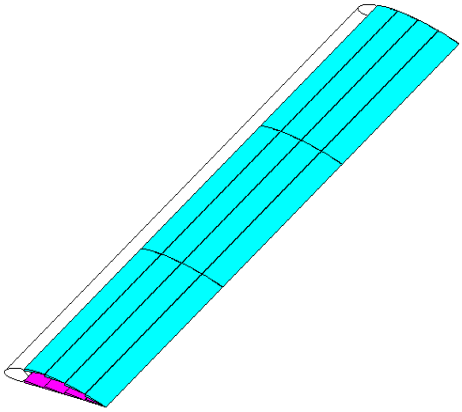

Figure 31: Rest configuration for cruise flight, all flap deflections are zero

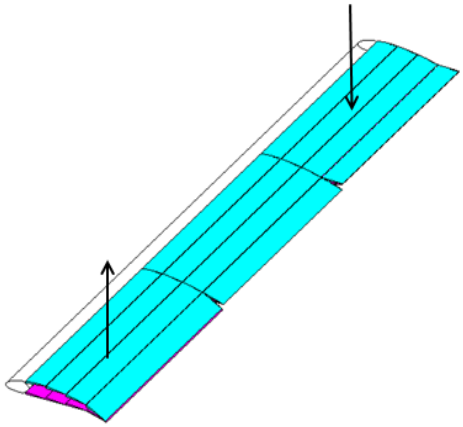

Figure 32: Clockwise roll,
$\delta_{11}=0°,\delta_{12}=0°,\delta_{13}=0°,\delta_{14}=-12°,\delta_{15}=0°,\delta_{16}=0°,\delta_{17}=0°,\delta_{18}=-14°$
$\delta_{21}=0°,\delta_{22}=0°,\delta_{23}=0°,\delta_{24}=0°,\delta_{25}=0°,\delta_{26}=0°,\delta_{27}=0°,\delta_{28}=0°$
$\delta_{31}=0°,\delta_{32}=0°,\delta_{33}=0°,\delta_{34}=14°,\delta_{35}=0°,\delta_{36}=0°,\delta_{37}=0°,\delta_{38}=12°$

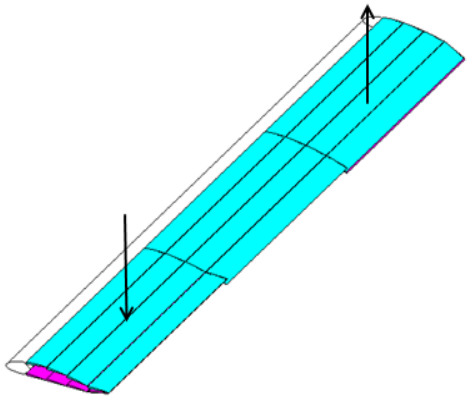

Figure 33: Counter- clockwise roll,
$\delta_{11}=0°,\delta_{12}=0°,\delta_{13}=0°,\delta_{14}=14°,\delta_{15}=0°,\delta_{16}=0°,\delta_{17}=0°,\delta_{18}=12°$
$\delta_{21}=0°,\delta_{22}=0°,\delta_{23}=0°,\delta_{24}=0°,\delta_{25}=0°,\delta_{26}=0°,\delta_{27}=0°,\delta_{28}=0°$
$\delta_{31}=0°,\delta_{32}=0°,\delta_{33}=0°,\delta_{34}=-12°,\delta_{35}=0°,\delta_{36}=0°,\delta_{37}=0°,\delta_{38}=-14°$

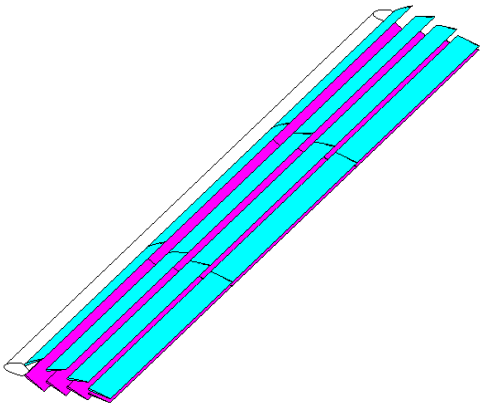

Figure 34: Air-Braking

When all flaps are deflected outwards into the airflow, the form drag on the wing increases resulting in air braking. The two-dimensional visualization of the counter-

rotating vortices is shown in Fig. 29, while the three-dimensional application is shown in Fig. 34.

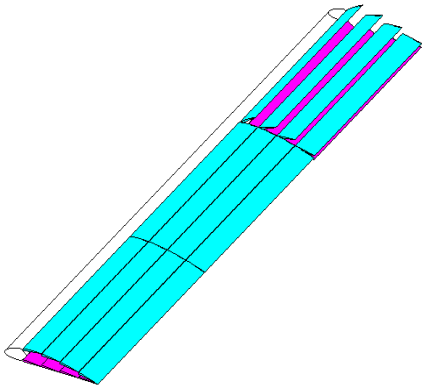

Figure 35: Right-Yaw

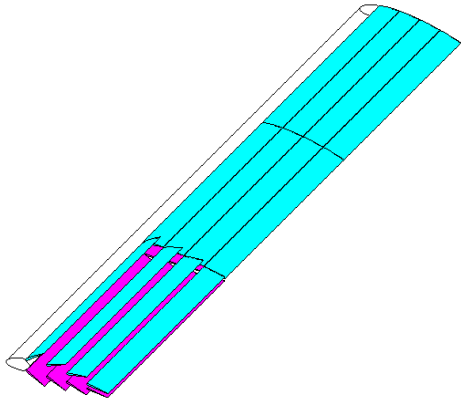

Figure 36: Left-Yaw

On the other hand, in the configurations shown in Figs. 35 and 36, the outward deflection of flaps only at either station 1 or 3 cause one side to undergo air-braking, causing yaw motion.

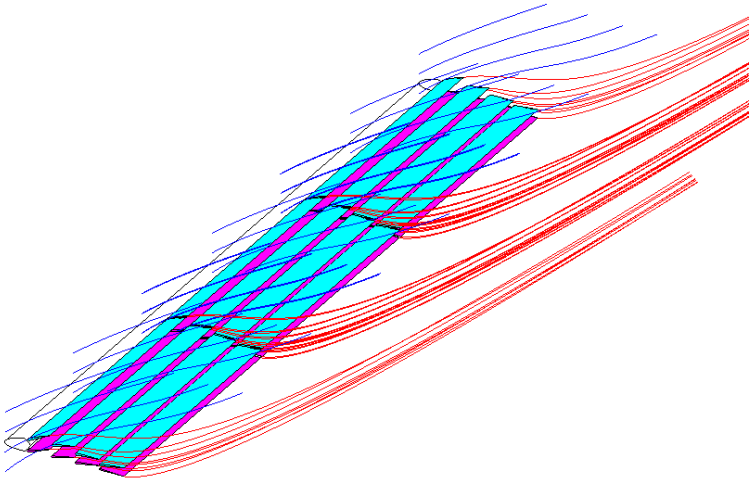

Figure 37: Gust Alleviation at high angle of attack.

When MFS wants to negotiate its path in gusting environment and maintain stability at a high angle of attack, the flaps can be deflected in the same direction to allow air to transpire through the structure. The deflection of flaps along the direction of the gust generates higher pressure gradients over the surface of the elements, which can oppose the adverse pressure gradient due to the skin friction. This avoids separation and increases the controllability of the wing.

Conclusion

Bio-inspired aerodynamics has paved the way for the development of more efficient and robust flight systems. The ability of morphing wings to adjust their shapes according to flight conditions not only improves the stability of an aircraft but extends its ability to fly in hostile and cluttered environments. With the increasing demand for better transportation, communication and unmanned aerial assistance in agriculture, construction, and media, it is imperative that novel and innovative flight mechanisms are developed and incorporated. The research undertaken in this thesis serves as an important step towards this development.

The increasing complexities in lifting surface geometries necessitate the development of better tools for their analysis. From an aerodynamic point of view, the development of the viscous-inviscid panel method undertaken in this thesis is an important stride towards the development of a rapid aerodynamic solver for preliminary design and analysis of multi-flap wings. The present solver is faster than commercially available software and is fairly accurate for low speed analysis. However, further improvement of the solver can be achieved by developing sub-routines to solve for high Reynolds number turbulent flows. This will make the solver more versatile, accurate and comparable to high fidelity CFD solvers.

The multi-flap design in itself can replace traditional control surfaces and improve the stability of a UAV. Not only does it preserve the integrity of standard airfoils, it adapts itself to unsteady flow conditions to provide better controllability and increase the

maneuverability of a bird-scale aircraft. The complete design can be retro-fitted on existing UAVs, which makes it more versatile and ubiquitous.

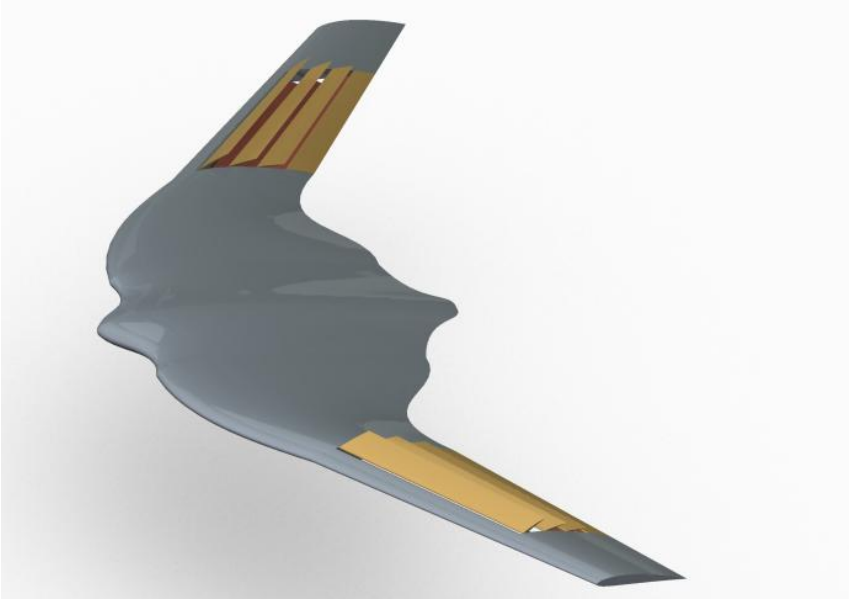

Figure 38: A UAV incorporated with the Bio-Inspired Multi-Flap System

One of the major challenges associated with such designs is the development of an autonomous control system to decide on a specific flap configuration when flight conditions drastically change. A distributed control system algorithm can be potentially incorporated but its design in itself is an arduous task. This thesis serves to establish a foundation to undertake such a complex research task. With a robust solver available for rapid analysis, an aerodynamic database can be easily created. This database then could be later used to design the control system.

With the increase in concern for human safety in industries such construction, wildlife surveillance and energy, the use of UAVs in domestic environments is almost inevitable. Thus, the need for smart and intelligent flight systems like the Multi-Flap System is not only essential but a requirement.

References

[1] Bone E., Bolkcom C., 2003, “Unmanned Aerial Vehicles: Background and Issues for Congress,” Report for Congress

[2] Williams W. and Harris M., 2002, “The Challenges of Flight-Testing Unmanned Air Vehicles,” in Systems Engineering, Test & Evaluation Conference, (October), Sydney, Australia

[3] P.A. Henne, Applied Computational Aerodynamics

[3] Blower C.J., Lee W., and Wickenheiser A.M., 2012 “The Development of a Closed-Loop Flight Controller with Panel Method Integration for Gust Alleviation using Biomimetic Feathers on Aircraft Wings,” in SPIE, pp. 1–13

[4] Blower C.J., Dhruv A, Wickenheiser A.M., 2014 " A Two Dimensional Iterative Panel Method and Boundary Layer Model for Bio-Inspired Multi-Body Wings." in SPIE 9055, Bioinspiration, Biomimetics, and Bioreplication 2014

[5] Blower, C.J., and Wickenheiser, A.M., 2012, “Two Dimensional Localized Flow Control Using Distributed Biomimetic Feather Structures: A comparative study"

[6] Dhruv Akash, Blower C.J., Wickenheiser A.M., 2014 " A Two Dimensional Iterative Panel Method and Boundary Layer Model for Bio-Inspired Multi-Body Wings.", SMASIS 2014

[7] Katz J and Plotkin A, Low-Speed Aerodynamics, 2nd ed., Cambridge University Press, New York (2001)

[8] Prof. Davenport Lectures, Aerodynamics, Virginia Tech

[9] Katz J, 1989, “Aerodynamics of High-Lift, Low-Aspect-Ratio Unswept Wings”, American Institute of Aeronautics and Astronautics, Volume. 27, Number.8

[10] Maskew B., “Program VSAERO Theory Document,” Redmond, WA (1987)

[11] Bramesfeld G., 2006, “A Higher Order Vortex-Lattice Method with a Force-Free Wake,” Pennsylvania State University.

[12] Basso D., 2013, “Improvement of a Low-Order Panel Method by Far-Field Computation of Induced Drag for Arbitrary Non-Planar Wing Configurations,” Universita Deglia Studi di Padovra .

[13] Sanderse B., 2008, "Cartesian grid methods for preliminary aircraft design.” TU Delft, Delft, Netherlands

[14] Ashby D.L., 1988 “Development and Validation of an Advanced Low-Order Panel Method”

[15] Johnson W., "Lifting-Surface Theory for Calculating Surface the Surface Loading Induced on a Wing by a Flap.” NASA Technical note, Ames Research Centre.

[16] Willis D.J., Peraire J, and White J.K., 2000, "A combined pFFT- multipole tree code, unsteady panel method with vortex particles wakes." International Journal of Numerical Methods in Fluids.

[17] David Joe Willis, "An Unsteady, Accelerated, High Order Panel Method with Vortex Particle Wakes", MIT, Boston, MA, June 2006.

[18] Winckelmans GS and Leonard A., "Contributions to Vortex Particle Methods for the Computation of Three-Dimensional Incompressible Unsteady Flows", Journal of Computational Physics 109, 247-273 (1993)

[19] Calabretta J.S. and McDonald R.A., "A Three Dimensional Vortex Particle-Panel Method for Modeling Propulsion-Airframe Interaction", *48th AIAA Aerospace Sciences Meeting Including the New Horizons Forum and Aerospace Exposition Proceedings: Orlando, Florida,* 2010

[20] Pinkerton P.M., NACA Report No. 613, "The variation with Reynolds Number of Pressure Distribution over an Airfoil Section."

[21] Turbulence Modeling Resource, Langley Research Centre, http://turbmodels.larc.nasa.gov/naca4412sep_val.html

[22] XFLR5 software http://www.xflr5.com/xflr5.htm

[23] Ali A.H., "Wake Roll-Up Behind Wings with Ground Effect," Iraqi Journal of Mechanical and Material Engineering 10(2), pp 181–202

[24] Moran J., 1984, An Introduction to Theoretical and Computational Aerodynamics, Dover Publications, New York.

[25] Blower C. J., and Wickenheiser A. M., 2013, "The Validation of a Generalized Aerodynamic Model for a Multi-Body Bio-Inspired Wing," Smart Materials, Adaptive Structures and Intelligent Systems, ASME, Snowbird, UT, pp. 1–11.

[26] Emre Alpman, "Airfoil Shape Optimization Using Evolutionary Algorithms", Pennstate University.

[27] Kelly Fleetwood, *An Introduction to Differential Evolution*

Appendix A - Differential Evolution Algorithm

Evolutionary algorithms have been widely used in engineering applications to obtain desired designs from a given set of parameters in the presence of multiple local minima. Differential evolution is essentially a cost-effective algorithm used to globally optimize a function. The algorithm takes a set of parameters influencing a function i.e. the design of the airfoil, and calculates best set of parameters between the given bounds for minimum cost [26-27].

To understand this in detail, considered the two designs of the leading edge of the Multi Flap System shown in Fig. 39. Since the leading edge and the outer surface of the MFS must follow a NACA 4412 geometry, the only varying parameters are the location of the trailing edge, the curvature of its rear part and the points on the upper and lower surfaces from which it starts to curve away from the NACA 4412 profile. The location of the trailing edge should vary between 0.06-0.09 times of the chord length to make sure that the trailing edge of the leading bluff body does not exceed the trailing edge of the first flaps. The maximum and minimum values of other parameters are shown in Table 1.

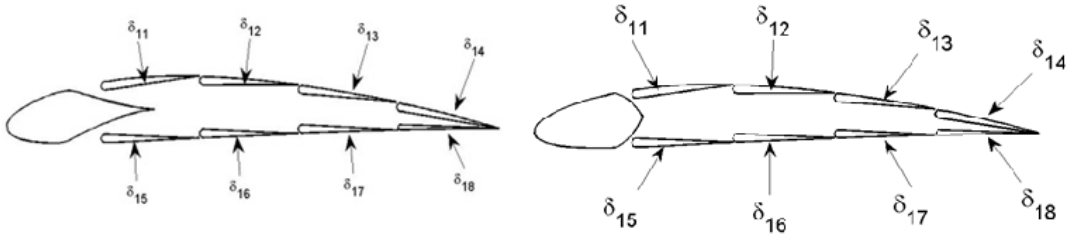

Figure 39: Different configurations of the leading edge of the Multi-Flap System

	T.E. Location	Upper Radius	Lower Radius
Upper Bound	(.09c, .01c)	.08c	.08c
Lower Bound	(.06c, .01c)	.05c	.05c
Optimized	(.07c,.01c)	.07c	.07c

Table 1: Design parameters of the leading edge

Once we have the upper and lower bounds of the parameters that define the geometry, we need to assign a cost function. In this case, the cost function is the error between the pressure distribution at the leading edge of a NACA 4412 airfoil and the Multi-Flap System, which needs to be minimized for an optimum design.

Differential Evolution:

Differential evolution consists of three sub-routines:

1. Mutation
2. Cross-over
3. Selection

Mutation

Using the upper and lower bounds of the design parameters, a set of initial guesses is generated by taking random values for each parameter between the bounds. These values are stored in an array x of size $D \times N_p$. Here, D is the total number of parameters that define the function. For example, in this case, the leading edge of the Multi-Flap System is defined by a set of 3 parameters and hence D = 3. $N_{p,}$ is the total number of initial guesses for a given parameter. For the algorithm to work successfully, the minimum value of N_p should be 4. This is because in each iteration a mutant array is generated using the initial array x, which is given by the equation,

$$v_{i,G+1} = x_{r_1,G} + F(x_{r_2,G} - x_{r_3,G}) \tag{40}$$

where, r_1, r_2, r_3 are random indices between *1-*N_p and should be different than the running index *i*. *G,* is the generation number that is essentially the loop counter for different designs. *F* is the mutation factor, which makes sure that the values calculated for the mutant vector do not match the values in the initial array. Its value ranges from 0 to 2.

Once the mutant array with a new set of design parameters is determined, the algorithm executes the sub-routine crossover. It is important to note that the size of array *v* is $D \times N_p$. This implies that the size of the mutant array for any given generation should be equal to the size of the initial array.

Cross-over

Cross-over increases the diversity of the perturbed parameters. This subroutine creates a trial vector

$$u_{i,G+1} = (u_{1i,G+1}, u_{2i,G+1}, u_{3i,G+1}, \ldots\ldots, u_{Di,G+1}) \tag{41}$$

such that

$$u_{ji,G+1} = \begin{cases} v_{ji,G+1} & \text{if } ran(j) \le CR \quad \text{or} \quad j = rnbr(i) \\ x_{ji,G+1} & \text{if } ran(j) > CR \quad \text{or} \quad j \ne rnbr(i) \end{cases} \tag{42}$$

where *ran(j)* is a uniform random number, *rnbr(i)* is a randomly chosen index which ensure that the trial vector gets at least one parameter from the mutated vector and *CR* is a crossover probability which taken as 0.9 [26].

Selection

In this sub-routine, the trial vector at generation *G+1* containing the design parameters is used to create a new leading edge design. This design is then solved for the aerodynamic coefficients. Once the results are available for this design, it is compared to the target design of NACA 4412. If the design in this generation is more cost-effective than the designs in the previous generation it is stored in the resultant array. At the end of all generations, the resultant array contains the most optimized design. The differential evolution algorithm proved to be a very important tool for the optimization of the leading edge.

A detailed discussion on the algorithm and its application to aerodynamic optimization can be found in [26-27].